Chemical Research in Toxicology

pubs.acs.org/crt

Article

Dissolution Rate of Nanomaterials Determined by Ions and Particle Size under Lysosomal Conditions: Contributions to Standardization of Simulant Fluids and Analytical Methods

Ilaria Zanoni, Johannes G. Keller, Ursula G. Sauer, Philipp Müller, Lan Ma-Hock, Keld A. Jensen, Anna Luisa Costa, and Wendel Wohlleben*

Cite This: *Chem. Res. Toxicol.* 2022, 35, 963−980

Read Online

ACCESS | Metrics & More | Article Recommendations | Supporting Information

ABSTRACT: Dissolution of inhaled engineered nanomaterials (ENM) under physiological conditions is essential to predict the clearance of the ENM from the lungs and to assess their biodurability and the potential effects of released ions. Alveolar macrophage (AM) lysosomes contain a pH 4.5 saline brine with enzymes and other components. Different types of artificial phagolysosomal simulant fluids (PSFs) have been developed for dissolution testing, but the consequence of using different media is not known. In this study, we tested to which extent six fundamentally different PSFs affected the ENM dissolution kinetics and particle size as determined by a validated transmission electron microscopy (TEM) image analysis. Three lysosomal simulant media were consistent with each other and with in vivo clearance. These media predict the quick dissolution of ZnO, the partial dissolution of SiO_2, and the very slow dissolution of TiO_2. The valid media use either a mix of organic acids (with the total concentration below 0.5 g/L, thereof citric acid below 0.15 g/L) or another organic acid (KH phthalate). For several ENM, including ZnO, $BaSO_4$, and CeO_2, all these differences induce only minor modulation of the dissolution rates. Only for TiO_2 and SiO_2, the interaction with specific organic acids is highly sensitive, probably due to sequestration of the ions, and can lead to wrong predictions when compared to the in vivo behavior. The media that fail on TiO_2 and SiO_2 dissolution use citric acid at concentrations above 5 g/L (up to 28 g/L). In the present selection of ENM, fluids, and methods, the different lysosomal simulant fluids did not induce changes of particle morphology, except for small changes in SiO_2 and $BaSO_4$ particles most likely due to ion dissolution, reprecipitation, and coalescence between neighboring particles. Based on the current evidence, the particle size by TEM analysis is not a sufficiently sensitive analytical method to deduce the rate of ENM dissolution in physiological media. In summary, we recommend the standardization of ENM dissolution testing by one of the three valid lysosomal simulant fluids with determination of the dissolution rate and halftime by the quantification of ions. This recommendation was established for a continuous flow system but may be relevant as well for static (batch) solubility testing.

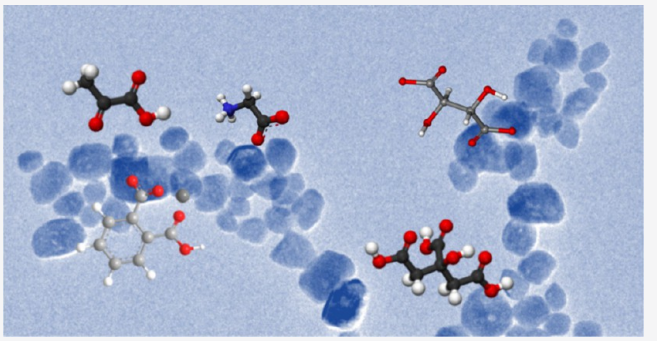

INTRODUCTION

The health effects of inhaled engineered nanomaterials (ENM) depend strongly on their biodurability and elimination from the lungs, that is, the biological lifetime within which these materials might elicit adverse effects. The abiotic dissolution rate is considered an appropriate parameter to assess the biodurability of fibers or particles, and it can be assessed in either static or dynamic flow-through test systems.[1−4]

Traditionally, acellular testing of the dissolution rates of inhalable minerals and fibers has been conducted at two pH values: pH 7.5 to reflect the near-neutral extracellular lung fluid and pH 4.5 to reflect the acidic intracellular environment of alveolar macrophage (AM) lysosomes.[1,2,5] Generally, silica and glass wool fibers are relatively more soluble at pH 7.5 than at pH 4.5,[6] whereas most carbonates, sulfates, oxides, and stone wool fibers are more soluble at pH 4.5 than at pH 7.4.[6−10] In addition to dissolution and solubility, pH also affects the leaching of specific elements from a material.[11]

Over time, a variety of lung-lining and lysosomal simulant fluids containing different salts and organic compounds have been used for dissolution testing with various levels of justification.[2,6] For man-made fibers, a de facto industry standard existed since 2002,[12] but it is currently being debated for potential revision.[13] In general, and specifically for ENM,

Received: December 2, 2021
Published: May 20, 2022

experimental evidence is lacking on the appropriate composition for an extraction fluid reflecting AM lysosomes.[14] Such fluids can be used on several different setups, for example, in stirred beaker setups or continuous flow systems, as described in the International Organization for Standardization (ISO) Technical Report (TR) 19057.[15] An Organisation for Economic Co-operation and Development (OECD) Guidance on methods to determine solubility and dissolution rate is currently being developed.[16]

A historical comparative study on several mineral fibers demonstrated a dramatic (more than 100-fold) influence of the exact composition of the pH 4.5 fluid on the fiber dissolution rates.[17] Studies have also shown up to 20 differences in dissolution rates in tremolite depending on the concentrations of organic ligands.[18] We recently reproduced these historical results on modern mineral fibers and additionally demonstrated the strong modulation of the transformation of physical structures and reprecipitation phenomena by the different pH 4.5 extraction fluids.[19] However, the narrowly defined composition of mixed-oxide mineral fibers and the modulation by their organic binder coating make it impossible to extrapolate the results to the much wider diversity of ENM compositions.

The present study aims to support the standardization of ENM dissolution by recommendation of valid pH 4.5 simulant media. We pursue a pragmatic approach to substantiate the selection of a pH 4.5 extraction fluid that is considered suitable in reflecting the environment present in AM lysosomes:

- First, available information on the composition of macrophage lysosomes is summarized.
- Second, the composition of pH 4.5 extraction fluids reported in peer review studies is comparatively assessed. Thirteen relevant media with varying compositions were found. However, only six of them varied significantly in composition. The other media were related to this selection with no or only minor differences in composition.
- Third, the dissolution of ENM is experimentally determined in an identical setup and with a standard operative procedure (SOP) using different phagolysosomal simulant fluids at pH 4.5 that represent the diversity of simulants used in the literature. The used media were chosen based on difference in the salt concentration, differences in the identity and concentration of organics (especially organic acids), differences of acids and bases: phthalate,[17] citrate, and HCl,[20,21] and the media that were previously thoroughly tested.[22] To determine the span of relevant ENM biopersistence, we performed the experimental testing on:
- CeO_2 NM-212 (in vivo very low dissolution)
- TiO_2 NM-105 (in vivo very low dissolution)
- $BaSO_4$ NM-220 (in vivo partial dissolution and partial transformation)
- SiO_2 NM-200 (in vivo partial dissolution)
- ZnO NM-111 (in vivo quick dissolution and coated)

We quantified the dissolution kinetics via ICP-MS of the eluted ions and prepared the remaining solids onto TEM grids. In this manner, we can both draw conclusions on the validity of simulant fluids and recommend the methodology for the detection and quantification of dissolution rates and halftimes.

RESULTS OF LITERATURE REVIEW

Composition of Macrophage Lysosomes. Macrophage lysosomes are a central organelle in the processing of exogenous and intracellular biomolecules.[23] Rich in hydrolytic enzymes, lysosomes are responsible for the phagocytosis and endocytosis of macromolecules from the extracellular environment or for their autophagy from the cytosol. Within the lysosomes, the macromolecules are degraded for reutilization.[24] Furthermore, lysosomes are involved in specialized functions such as antigen presentation and the regulation of growth factors and hormones.[24] The acidic pH present in lysosomes under different experimental conditions has been a matter of extensive investigations.[24−27]

Overall, relevant peer review studies that report on constituents of (alveolar or other) macrophage lysosomes appear scant. The reviewed literature does not yield comprehensive information on the precise organic and inorganic constituents of macrophage lysosomes.

Due to the overall paucity of relevant information, studies were also included in the evaluation if they addressed lysosomes from tissues other than the lungs and from cells other than macrophages. However, lysosomes from different cell types do not necessarily have the same constituents. Weber and Schilling[28] showed considerable baseline differences in lysosome morphology and functions between peritoneal macrophages (PMs) and bone marrow-derived macrophages (BMMs) isolated from thioglycolate-treated C57BL/6 mice as evidenced by immunofluorescence imaging and gene and protein expression analyses:[28]

> *Consistent with the flow cytometry and imaging data, the expression of genes encoding cathepsin proteases, lysosomal membrane proteins, and the vacuolar ATPase was increased in PMs relative to BMMs... the autophagy related genes LC3 and p62 were also expressed at a higher level in PMs.... Thus, mRNA expression of lysosome and autophagy related genes is increased in PMs, which is likely related to the expanded lysosome compartment observed in these primary macrophages. At the protein level, pro-cathepsin D protein content was increased in PMs relative to BMMs.... [Similarly] lysosomal membrane-associated glycoprotein 1 (LAMP1) protein content trended towards an increase in PMs compared to BMMs... the molecular weight of LAMP1 was significantly greater in BMMs suggesting a higher level of glycosylation, a finding which could further affect lysosome function and stability in these two types of primary macrophages.*[28]

We are unaware of similar comparative studies including AMs (note that LAMP1 and LAMP2 are considered major constituents of lysosomal membranes).[29]

Of the documents retrieved, the book chapter "*Lysosomal enzymes and other components*" by Tappel provided the most comprehensive information on lysosome composition—while not focusing on AMs but on liver and kidney cell lysosomes.[30] Relevant information from this chapter is summarized below:

> *The known constituents of lysosomes include hydrolytic enzymes, structural lipids and proteins of the membrane, products of hydrolysis which accumulate in the lysosomes, and cellular parts and macromolecules which have yet to be digested or which resist digestion.*[30]

Enzymes found in lysosomes include proteases and peptidases, nucleases, enzymes hydrolyzing the carbohydrate chains of glycoproteins and glycolipids, and enzymes degrading

https://doi.org/10.1021/acs.chemrestox.1c00418
Chem. Res. Toxicol. 2022, 35, 963−980

Table 1. Overview of Lysosomal Enzymes with pH Optima at Approximately pH 4.0−4.8 and Other Components as Recorded by Tappel, Adapted from ref 30

enzyme family	enzyme	substrate specificity	pH optima	experimental substrate/enzymic source	major natural substrates
nucleases	acid deoxyribonuclease	phosphodiester linkages of DNA	4.5	DNA/spleen	DNA
phosphatases	acid pyrophosphatase	flavin adenine dinucleotide, ATP	4.0	ATP and flavin adenine dinucleotide/liver lysosomes	flavin adenine dinucleotide and ATP
enzymes hydrolyzing the carbohydrate chains of glycoproteins and glycolipids	*β*-*N*-acetyl hexosaminidase	*β*-*N*-acetyl glucosaminides *β*-*N*-acetyl galactosaminides	4.0−4.6	nitrophenyl-*β*-*N*-acetyl glucosaminide/liver lysosomes	*β*-*N*-acetyl hexosaminides in glycoproteins and glycolipids
	α-*N*-acetyl hexosaminidase	*α*-*N*-acetyl glucosaminides *α*-*N*-acetyl galactosaminides	4.5	nitrophenyl-*α*-*N*-acetyl glucosaminide/testis	heparan sulfate
	α-mannosidase	*α*-mannosides and related glycosides	4.6−5.0	not recorded	*α*-mannosides in glycoproteins
	sialidase	sialic acid derivatives	4.0−4.4	sialyllactose and glycoprotein/liver and kidney lysosomes	glycoproteins and glycolipids
	O-seryl-*N*-acetyl-galactosaminide glycosidase	seryl acetyl galactosaminide	4.4	submaxillary gland glycoprotein/kidney and liver lysosomes	seryl acetyl galactosaminide in glycoproteins
enzymes degrading glycosaminoglycans	*β*-glucuronidase	all aliphatic and aromatic *β*-D-glucosiduronic acids	4.5−5.2	phenolphthalein *β*-glucuronide/liver lysosomes	polysaccharides, mucopolysaccharides, and steroid glucuronides
	arylsulfatase A	nonspecific, aryl sulfates	4.9	nitrocatechol sulfate/liver	aryl and cerebroside sulfates, chondroitin 4-sulfate
enzymes degrading lipids	triglyceride lipase	triglycerides	4.2	glycerol tridecanoate/liver and kidney lysosomes	triglycerides
	phospholipase	phospholipids	4.5	lecithin, lysolecithin, and phosphatidyl ethanolamine/liver lysosomes	lecithin, lysolecithin, and phosphatidyl ethanolamine
	esterase	fatty acid esters	3.6−4.0	fatty acid esters of *p*-nitrophenol/liver and kidney lysosomes	fatty acid esters

https://doi.org/10.1021/acs.chemrestox.1c00418
Chem. Res. Toxicol. 2022, 35, 963−980

glycosaminoglycans or lipids. Tappel[30] also reports on the location of the enzymes within the lysosomes:

> *Some of the hydrolytic enzymes are readily solubilised by physical treatment and are probably located in the interior of the lysosome. Other hydrolases cannot be solubilised and are probably bound to the unit membrane.*

The pH optima of the different lysosomal enzymes encompass a broad range of pH values, for example, for the family of proteases and peptidases, the range is from pH 2.5 for cathepsin E to pH 7.8 for peptidase.[30] Table 1 in the annex to this briefing presents those lysosomal enzymes for which Tappel recorded a pH optimum of 4.0−4.9. Tappel[30] also listed the specific activities of these enzymes, recording very high specific activities in rat liver lysosomes (>200 μmol substrate hydrolyzed/min/kg protein) for cathepsin C and D, dipeptidase (tyrosyl-glycine), acid phosphatase, acid pyrophosphatase, β-*N*-acetyl glucosaminidase, esterase, and phosphatase.

Tappel[30] further found 5−10 times higher concentrations of free amino acids in the lysosomal fraction of rat liver and kidney tissues than in whole liver homogenates. This difference was particularly relevant for leucine (the most abundant amino acid in lysosomes), isoleucine, alanine, and threonine.

Finally, Tappel[30] reported phospholipids (lecithin, phosphatidylethanolamine, and inositol phosphatide) and different fatty acids and flavins as being present in lysosomes. Of the metals, Fe, Cu, Mn, Zn, and Mo were found in lysosomes via spectrography at 2.00, 0.10, 0.03, 0.30, and 0.01 mg/g protein, respectively. Additional metals below the detectable level of 0.0003 mg/g protein included cobalt, chromium, and vanadium. Tappel noted that the most abundant metal, Fe, was likely present in the lysosomes as ferritin and that metal concentrations in lysosomes were higher than in the mitochondria and microsomes.[30]

Arborgh et al.[31] isolated Kupffer cell lysosomes from rats pretreated with intravenous injections of colloidal silver iodide.[31] Silver concentrations in the Kupffer cell lysosomes were highest 1 h after treatment, but the activities or distribution of acid phosphatase, aryl sulfatase, or cathepsin D remained unaffected. As compared to the whole liver homogenate or microsomal fraction, the lysosomal fraction exhibited very low concentrations of protein, phospholipids, and cholesterol.

Berry performed electron probe X-ray microanalysis of ex vivo ultrathin tissue slices to investigate how lysosomes contributed to the cellular uptake of diverse elements.[32] The findings showed that 21 elements in soluble form, injected intraperitoneally or intravenously into rats, were selectively concentrated within the lysosomes of a spectrum of cells including BMMs, lymph node macrophages, hepatocytes, and renal tubular cells. Fifteen of the 21 elements precipitated in the lysosomes in association with phosphorus, whereas the other six precipitated in association with sulfur. The 15 elements which precipitated with phosphorus in lysosomes included three group III-B elements of the periodic system (aluminum, gallium, and indium), rare-earth elements (cerium, gadolinium, lanthanum, thulium, and samarium), two group IV-A elements (hafnium and zirconium), two actinides (uranium and thorium), chromium, and niobium. The six elements that precipitated with sulfur comprised of three group VIII elements (nickel, palladium, and platinum) and three group I-B elements (copper, silver, and gold). Berry[32] concluded that these processes were driven by enzymatic processes involving acid phosphatases for elements precipitating as phosphates and arylsulfatases for elements precipitating as sulfates.

Single studies have addressed the presence of individual inorganic compounds in lysosomes:

Christensen et al. used mouse BMMs to assess how extracellular calcium changes affected the lysosomal pH, and, vice versa, how alterations in the lysosomal pH affected lysosomal calcium concentrations.[33] The authors concluded that:

> *Lysosomal calcium concentration is high and is maintained in part by the proton gradient across lysosomal membranes. Moreover, lysosomes could provide an intracellular source for physiological increases in cytosolic calcium levels.*[33]

Köpf-Maier investigated the phosphorus content of lysosomes in hepatocytes and Kupffer cells and found that the lysosomes of Kupffer cells always comprise phosphorus in high density, whereas the hepatocyte lysosomes did not. Köpf-Maier concluded that the elemental composition of lysosomes in hepatocytes and Kupffer cells exhibited a pronounced and unexpected heterogeneity.[34]

Tapper and Sundler assessed how different agents affecting intracellular pH influenced the secretion of lysosomal β-*N*-acetyl hexosaminidase and preloaded fluorescein-labeled dextran from cultured mouse PMs. Nigericin raised the lysosomal pH in both K^+- and Na^+-based media. The increases were more pronounced in the K^+-based medium and occurred at lower concentrations than effects induced by monensin.[35]

Rider et al. applied cytochemistry and autoradiography to characterize the role of rabbit lung cell lysosomes in the catabolism of a radio-labeled dipalmitoyl phosphatidylcholine surfactant applied via intratracheal instillation. The study showed that surfactants accumulated in the lysosomes, and the arylsulfatase B activity in the lysosomes increased.[36]

Further studies addressed how particles were taken up into lysosomes. While these studies confirm that lysosomal particle uptake and dissolution are relevant aspects of inhalation toxicity, they also do not provide information on the composition of AM lysosomes.

- Lundborg et al. assessed how the AM phagolysosomal morphology changed upon exposure to cobalt oxide particles.[37,38]
- Oh and Swanson assessed the fate of phagocytosed polystyrene particles after delivery into BMM lysosomes.[39]
- Berry et al. showed that inhaled soluble elements are concentrated in rat AM lysosomes, precipitating as insoluble phosphates. Small crystals of inhaled crystalline poorly soluble particles were captured in AM lysosomes and gradually transformed into amorphous forms.[40]
- Wan et al. showed that acid-functionalized single-walled carbon nanotubes (SWCNTs) and graphene oxides accumulated in PM lysosomes, leading to lysosome membrane destabilization and reduced autophagic degradation.[41]

In summary, we were unable to find comprehensive information on the inorganic constituents of AM lysosomes. Apparently, while the enzymes and proteins that comprise the lysosomal fluid are widely known, but not constant and not easily reproduced, comprehensive ionic composition data remain unavailable.[2,22]

Composition of pH 4.5 Extraction Fluids Reported in the Literature. We analyzed the compositions of pH 4.5 extraction fluids reported by different research groups.[1,17,19−22,42,43] Thirteen relevant media with varying

https://doi.org/10.1021/acs.chemrestox.1c00418
Chem. Res. Toxicol. 2022, 35, 963−980

compositions were found. However, only six of them varied significantly in composition (Table 2). The other media were related to this selection with no or only minor differences in composition (Table SI_1) based on differences in the salt concentration, differences in the identity and concentration of organics (especially organic acids), and differences of acids and bases.

Kastury et al. summarize how the different pH 4.5 extraction fluids were developed:[2]

> *...researchers initially adjusted the pH of Gamble solution[15] to 4.5 by adding hydrochloric acid or using buffers (Guldberg et al.[17]). Thelohan and De Meringo[46] formulated a more complex simulated AM fluid with a similar ionic composition to extracellular fluid. This fluid was termed 'simulated intracellular fluid' or 'acid solution'. Turner et al.[43] adapted this composition by substituting glycerine for glycine, which became known as the artificial lysosomal fluid (ALF), without justifying this substitution. Midander et al.[21] adapted this ALF formulation by omitting formaldehyde and glycerine and including glycine. This composition is now widely accepted and used in most inhalation studies to represent the conditions under which metal dissolution occurs inside the lysosome of AMs. A fourth formulation of the AM fluid was devised by Stefaniak et al.,[22] with fewer organic components, while keeping similar ionic concentration. This formulation became known as PSF. Glycine was added to this solution to represent all organic acids and potassium hydroxide (0.1 M) was included to maintain the pH at 4.55.*[2]

Kastury et al.[2] further highlighted limitations to "method parameters (extraction time, solid to liquid ratio, temperature and agitation) that are often not biologically relevant".[2] Few studies address how individual components of extraction fluids affect dissolution rates. Zoitos et al. highlighted that the use of extraction fluids with low Ca concentrations enabled the measurement of Ca dissolution in addition to Si dissolution.[44] Li et al. measured the dissolution of biotite and observed that K, Si, and Al release rates increased when citric acid was added to pH 4 solutions.[45] High concentrations of citric acid are included in the pH 4.5 extraction media reported by Stopford et al., Midander et al., and Shinohara et al.[21,42,43] In contrast, the media reported by Thelohan and De Meringo and Stefaniak et al. are devoid of citric acid.[22,46]

Liu et al. studied the dissolution rates of SWCNTs in PSF[47] by further adding 1 mM H_2O_2 and compared the findings to those from Allen et al.,[48] suggesting that both studies report the structural degradation of carboxylated nanotubes, if oxidizing acid mixtures are present such as H_2SO_4/H_2O_2 or HNO_3. Similarly, Russier et al. compared the structural biodegradation of SWCNTs and multiwalled carbon nanotubes (MWCNTs) in PSF supplemented with H_2O_2 to biodegradation upon addition of horseradish peroxidase and H_2O_2.[49] However, in both these studies, other phagolysosomal contents were not included.

Recently, Yokel et al. assessed how the dissolution of nanosized CeO_2 dispersed in an aqueous environment (pH 4.5) containing citric acid as a stabilizing agent was affected by the addition of 10 different carboxylic acids (including lactic acid, DL-malic acid, succinic acid, citric acid, acetic acid, glutaric acid, and tricarballylic acid).[50] Dissolution was generally low but measurably different depending on the added acid. Upon addition of lactic acid, nano-CeO_2 completely dissolved within 18 weeks. Addition of the nine other acids for 28 weeks yielded average CeO_2 diameters ranging from 1.70 nm (DL-malic acid) to 3.30 nm (tricarballylic acid; by comparison: 4.17 nm upon 28-week incubation in water). Even though the acids were added at high acid concentrations exceeding physiologically relevant ranges,[50] the findings show that different organic acids can affect material dissolution properties to different extents.

While enzymes and proteins are pivotal constituents of AM lysosomes, none of the pH 4.5 extraction fluids that we found in the literature included proteins. As discussed by Boisa et al.,[14] citing Marques et al.:[51]

> *Typical recipes for synthetic lung fluids indicate sufficient salt (mineral) content but appear to be deficient in representing the mix of organic molecules in the native respiratory tract environment.*[14]

Regarding nanomaterial testing, the ISO/TR 19057 notes that simulated physiological fluids (SPFs):

> *...all suffer from the same basic limitations. Firstly, SPFs have defined compositions and lack the dynamic conditions present in vivo. For example, none of these fluids contain enzymes or oxidative cascades which can be important in dictating the properties (composition, pH) of a SPF or biodurability [...]. Additionally, unless specifically noted, proteins are omitted from most SPF for pragmatic reasons [...]; however, in vivo, proteins might serve as important binding molecules for dissolved ions and influence their concentration at nanomaterial surfaces (ISO/TR 19057).*[15]

Oberdörster and Kuhlbusch[3] discussed these limitations of simulant fluids with respect to the testing of metal compounds:

> *It is not known as to whether the lack in simulant fluids of specific proteins and other components, existing in vivo, cause significant differences between in vitro and in vivo results. There are no data to compare dissolution of the same metal compounds when using differing fluid compositions. Studies comparing the importance of the individual constituents of fluid simulants need to be designed. Even with that knowledge though, it remains to be determined as to whether and how specific metal ions interact with respiratory tract tissues. More studies/data are needed to accept static or dynamic acellular in vitro solubility/dissolution assays as standards.*[3]

We found two studies in which amino acids or proteins were added to extraction fluids, but neither study addressed dissolution at pH 4.5:

Boisa et al. presented the formulation for a pH 7.5 simulated epithelial lung fluid containing albumin, cysteine, dipalmitoyl phosphatidyl choline, glycine and mucin, ascorbic acid, uric acid, and glutathione in addition to different inorganic phase reagents.[14] This extraction fluid was the only medium used for assessing the biodissolution of <10 μm Pb in a range of urban surface soils and mining wastes. Therefore, the dissolution rates recorded by Boisa et al.[14] cannot be compared to data obtained using extraction fluids that are devoid of amino acids.

Walczak et al. presented an in vitro human digestion model simulating the oral, gastric, and intestinal compartments that contained both salt and protein and assessed 60 nm Ag nanoparticles (NPs) and silver ions ($AgNO_3$) in this model.[52] The findings showed that the Ag NPs were able to reach the intestinal wall in their original size if proteins were present in the simulation fluids.

In summary, a variety of different pH 4.5 extraction fluids simulating AM lysosomes are reported in the literature. All extraction fluids are composed of different inorganic compounds and—mostly high concentrations of—organic compounds. Variations between different fluids are often only slight and

https://doi.org/10.1021/acs.chemrestox.1c00418
Chem. Res. Toxicol. 2022, 35, 963−980

Table 2. Media Representing the Diversity of pH 4.5 Lysosomal Simulant Fluids Used for Testing in This Study[a]

	Guldberg et al.[17]			Muhle et al.[20]	Midander et al.[21]	Stefaniak et al.[25]
	C: MK (phthalate)	D: MG (citrate)	E: MG (HCl)			PSF
$MgCl_2$ * 6 H_20		0.106	0.160	0.106		
$MgCl_2$					0.0497	
NaCl	6.65	3.208	6.171	3.208	3.210	6.650
NaOH		1.888			6.000	
KCl			0.031			
$CaCl_2$ * 4 H_2O				0.159		
$CaCl_2$ * 2 H_2O	0.029	0.128	0.060	0.159	0.128	0.029
NH_4Cl	0.535					
Na_2SO_4 (anhydrous)	0.071	0.040	0.080		0.039	0.071
Na_2SO_4 * 10 H_2O				0.090		
Na_2HPO_4	0.171	0.074	0.148	0.074	0.071	0.142
$NaHCO_3$			1.900			
$NaCH_3CO_2$ * 3 H_20	0.954					
Na_2-tartrate * 2 H_2O		0.090	0.180	0.090	0.090	
citric acid					20.800	
citric acid * H_2O		5.424				
Na_3-citrate * 2 H_2O	0.059	0.076	0.152	5.313	0.077	
90% lactic acid		0.079	0.056			
Na-lactate				0.088	0.085	
glycine	0.450	0.059	0.118	0.059	0.059	0.450
KH-phthalate	2.043					4.085
Na-pyruvate		0.086	0.172	0.086	0.086	
HCl			0.881			

[a]All values are given in g/L.

generally not justified. An excellent review with critical discussion of the role of salts, organic components, and pH ranges was provided by Innes et al., which supports our conclusions.[6] The added organic compounds, specifically the organic acids meant to represent enzymes, can stabilize dissolved components, thereby shifting their dissolution toward faster rates.

EXPERIMENTAL TESTING

Study Design, Materials, and Methods. We tested the dissolution of ENM in an identical setup and SOP using different phagolysosomal simulant fluids at pH 4.5 that represent the diversity of simulants used in the literature (Table 2). The selected ENM test materials were provided by the Fraunhofer Institute and the JRC Repository and have been extensively characterized previously. A summary is given in Table SI_2, which is reproduced from Llewellyn et al.[53] To determine the span of relevant ENM biopersistence, we performed the experimental testing on five ENM representing different dissolution behaviors and pulmonary clearance rates as observed from in vivo inhalation studies:

- CeO_2 NM-212 (very slow clearance rate)
- TiO_2 NM-105 (very slow clearance rate)
- $BaSO_4$ NM-220 (partial dissolution, partial transformation, and intermediate clearance rate) (containing on the surface 1.8% organics as processing aid[54,55])
- SiO_2 NM-200 (partial dissolution and intermediate clearance rate)
- ZnO NM-111 (quick dissolution and fast clearance rate) (coated by 3.5% triethoxycaprylsilane as hydrophobisation[55,56])

The composition of NM-200, which is Synthetic Amorphous Silica, is approximated here as SiO_2.

Determination of the Dissolution Rate and Halftime by the Quantification of Ions. The setup was a continuous flow system (CFS) as described in several recent studies.[57−59] In short, the ENM were held between membranes of a flow cell such that ions are continuously removed by a fluid flow that was previously validated by comparison of measured halftimes to in vivo inhalation results of particles[59] and fibers.[12] All method-related parameters were held constant:

- Initial ENM mass: 1 mg, which was measured using a microbalance with a sensitivity of 0.01 mg.
- Fluid flow: 2.0 ± 0.2 mL/h (fresh simulant flowing through the cell and into 5 mL samplings).
- Temperature: 37.0 ± 0.1 °C.
- Flow-through membrane: 5 KDa cellulose triacetate (Sartorius, part no.: 14529-47-D, cutoff ca. 1.1 nm), 47 mm diameter.
- Duration of measurement: 7 days.

A PerkinElmer NexION 2000 was used for elemental analysis. All samples were stabilized with 1% (v/v) HNO_3 and were diluted to ensure that the samples did not exceed the detection limits of the instrument. We measured with kinetic energy discrimination (KED)

https://doi.org/10.1021/acs.chemrestox.1c00418
Chem. Res. Toxicol. 2022, 35, 963−980

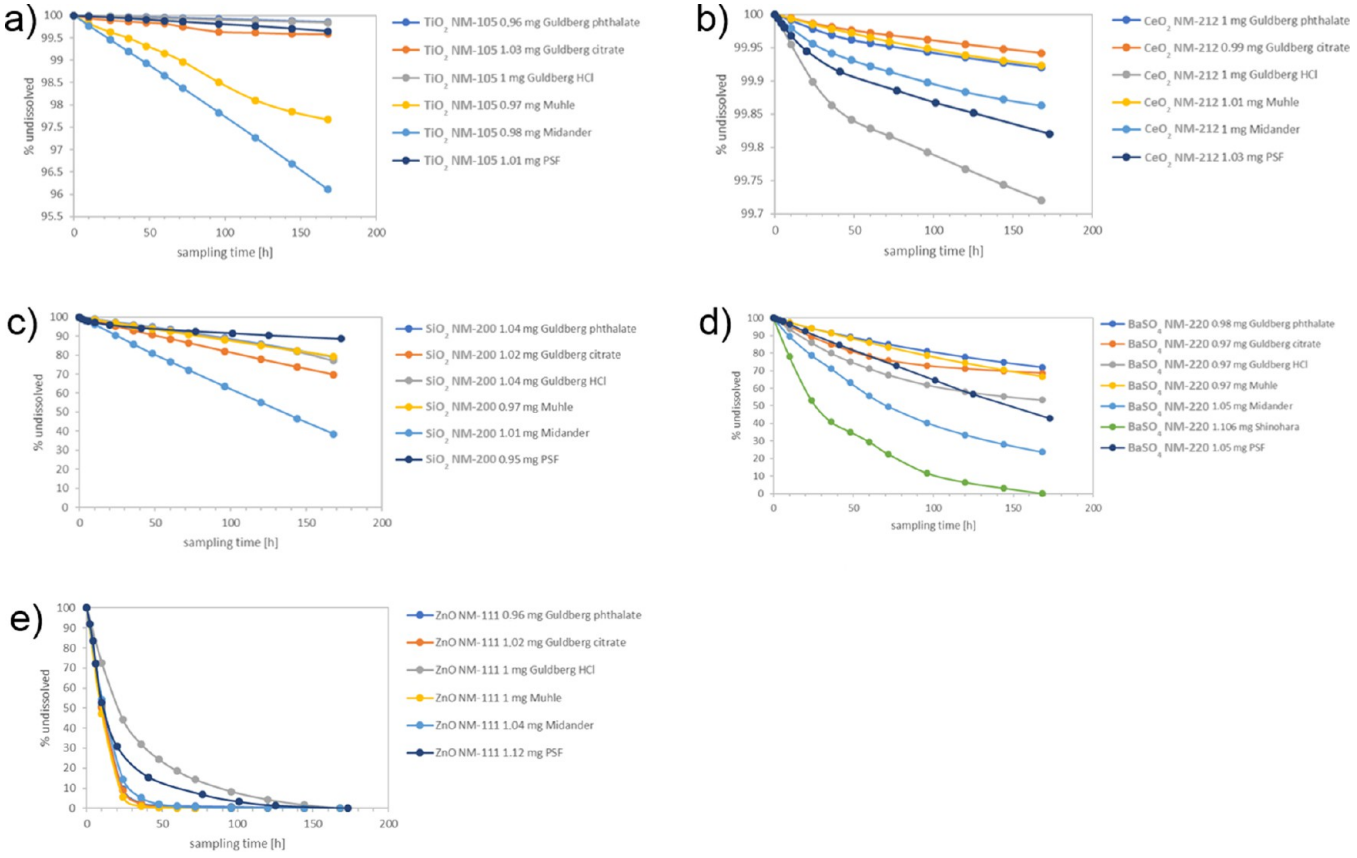

Figure 1. Concentration−time plot of five ENM in six media. (a) TiO_2 NM-105, (b) CeO_2 NM-212, (c) SiO_2 NM-200, (d) $BaSO_4$ NM-220, and (e) ZnO NM-111. Concentration is given in wt %.

with helium gas and used ^{45}Sc as an internal standard. Calibration curves for each analyte were used and verified during each run to obtain the concentration values. Ce, Ti, Zn, and Ba had a limit of detection (LoD) of 0.1 μg/L with an external calibration of 0.1/1/10/100/1000 μg/L (ppb). For Si, the LoD was 1 μg/L with an external calibration of 1/10/100/1000 μg/L (ppb) in the KED mode. The integration time was 50 ms, and the argon flow of the Meinhard nebulizer was 0.92 L/min. The dissolution rates were determined between each successive sampling, resulting in 10 values per material and fluid, which were averaged.[60] The stepwise calculation is detailed in the Supporting Information. Independently, an intralab validation with the PSF fluid on TiO_2 and ZnO with each n = 5 cells had been performed. It demonstrated that the dissolution rate k was reproducible at 40% relative error across a dynamic range from below 0.01 to above 500 ng/cm^2/h. The fitted halftime was reproducible at 40% relative error for slow dissolution but at 20% relative error for fast dissolution. These results for nanomaterial dissolution confirmed the earlier findings of a relative error of 24 to 61% reported by two earlier interlab comparisons on dissolution with CFS on mineral fibers.[61] The assessment of measured dissolution rates would thus consider a twofold difference as significant.

Assessment of the Particle Size and Shape. By the preparation of TEM grids after the 7-day dissolution and their analysis by TEM, we explored the extent to which different media induce different transformations. The methodology followed exactly the protocol that Keller et al. had successfully used to identify the transformation of $BaSO_4$ NM-220 via Ostwald ripening, where the abiotic method was confirmed by the in vivo inhalation with high-resolution TEM images of lung slices.[58] In short, the remaining solids inside the flow cell at the end of the 7-day dissolution testing were flushed by DI water and then pelleted onto a TEM grid by centrifugation at 49.000g for 2 h. Under these conditions, the density dictates the diameter of the smallest particles that are quantitatively transferred onto the grid: 9 nm (silica), 4.5 nm (ZnO), 4 nm (CeO_2), 6 nm (TiO_2), and 5.3 nm ($BaSO_4$). Even smaller particles would still be present but they were underrepresented on the grid. The grids were analyzed by TEM and evaluated using an automated image analysis with the interlab-validated NanoDefine algorithm.[62,63] The FEI EM208 instrument operated a Schottky FEG at 200 kV (Philips, Eindhoven, The Netherlands) with a high-definition acquisition system based on a side-mounted OSIS Morada TEM camera and an iTEM software platform (Olympus Soft Imaging Solutions GmbH, Münster, Germany).

Lysosomal Simulant Media. The used media were chosen based on difference in salt concentrations, differences in the identity and concentration of organics (especially organic acids), differences of acids and bases: phthalate,[17] citrate, and HCl,[20,21] and the previously thoroughly tested media.[22] Guldberg et al. named their fluids (E) "modified Gamble" (MG) (HCl), (C) "MK (phthalate)," and (D) "MG (citrate)." In these names, HCl, phthalate, and citrate refer to the acidifying agent.[17] Fluid E includes Na_2 tartrate, Na_3 citrate, lactic acid, and glycine; fluid C includes Na_3 citrate, glycine, and KH phthalate; and fluid D includes Na_2 tartrate, citric acid, glycine, and KH phthalate (Table 2). The same pH 4.5 simulant fluids have recently been compared with regard to the dissolution and transformation of stone wool fibers, in the same CFS, but with adjusted parameters (50 mg initial mass) to compensate for the lower specific surface area of mineral fibers.[19] The Muhle medium is almost identical to the medium (D) MG (citrate) and only uses different salts of the same organic acids. The Midander medium uses the highest concentration of an organic acid with 20.8 g/L citric acid (Table 2). The PSF medium is slightly simplified from medium (C) MK (phthalate) and uses only KH phthalate and glycine as organic components (Table 2).

RESULTS

Dissolution Kinetics Determined on Ions. The decrease of concentration versus exposure time for all media is shown in Figure 1. At each of their different levels of dissolution (note the

https://doi.org/10.1021/acs.chemrestox.1c00418
Chem. Res. Toxicol. 2022, 35, 963−980

different *y*-axes starting from 0% or from 99.7%), each of the ENM shows a modulation by the choice of the simulant medium. The results confirm previous evidence that the CFS method is capable to differentiate biodissolution halftimes across more than 3 orders of magnitude (Table 3): TiO_2 and CeO_2 have very slow $t1/2$ (>1000 days), whereas quick dissolution and short $t1/2$ (0.7 days) were observed for ZnO NM-111 (despite the coating). The $t1/2$ for SiO_2 NM-200 and $BaSO_4$ NM-220 was relatively fast intermediate as expected.

In order to highlight the modulation by the simulant medium, Figure 2 plots the normalized dissolution rates. A normalized plot of halftimes would look the same, and the *x*-fold ratio between the different simulant media would have the same numerical values. The dissolution rates measured in three of the media deviate by less than a factor of 2 between each other:

- Guldberg_phthalate (C: MK)
- PSF
- Guldberg_HCl (E: MG)

In the three abovementioned media, the biggest differences are observed for CeO_2 NM-212 and SiO_2 NM-200, dissolved in Guldberg HCl at 150 and 205% of their respective rates in PSF, and again SiO_2 NM-200 dissolved in Guldberg phthalate at 190% of its rate in PSF, whereas all other materials in this medium dissolved around 50% of their rate in PSF.

However, for at least two materials (SiO_2 NM-200 and TiO_2 NM-105), the dissolution rates are up to 800% (eightfold) faster in the following three media than in the above group of media:

- Midander
- Muhle
- Guldberg_citrate (D: MG)

Based on these data, in the discussion section, we can identify valid and nonvalid media by the comparison against in vivo observations on identical materials, which were chosen because such data exist.

To investigate the role of the use of different acids further, dissolution of $BaSO_4$ was also tested in a seventh medium known as the Shinohara medium. The Shinohara medium was previously used to assess the dissolution of Ni-oxide ENM and contains 28 g/L citric acid (Table SI_1).[42] It was observed that $BaSO_4$ dissolved significantly even faster than in the Midander medium with 20 g/L citric acid and significantly faster than in any of the other media (Figure 1d, green line). Consequently, the Shinohara medium was not tested further on the other materials, which are known to be even more sensitive to excessive citric acid concentrations. The dissolution of the partially dissolving, partially transforming $BaSO_4$ was additionally analyzed by detailed trajectories of the kinetics at each sampling point (Figure 3). The reduction of the total surface area by dissolution is modeled here by a shrinking sphere model of average particle surface (SA) at a constant fluid flow (V), as guided by ISO 19057:2017. A perfect exponential decay at a constant dissolution rate per surface area would result in a horizontal line. This is approximately the case for the Shinohara, Midander, PSF, and Muhle media. However, in the Guldberg_HCl and Guldberg_citrate media, the kinetics decelerate over time and do not match the exponential decay, as can be seen also from the plots in Figure 1d.

Transformation Determined on Remaining Solids. The transformation work in PATROLS (Physiologically Anchored Tools for Realistic nanOmateriaL hazard aSsessment) focused on the five lysosomal pH 4.5 media that had not been investigated in this respect before, whereas transformation of

Table 3. Validity Check by In Vivo-Measured Clearance,[54,69−72] which Is Converted to the Contribution of Dissolution to Clearance, which Is Then Compared to the Measured Dissolution Halftimes ($t1/2$) from CFS Dissolution in the pH 4.5 PSF Medium[a]

	derivation of $t1/2_{dissolution}$ (days) from in vivo studies				$t1/2_{dissolution}$ (days) measured by CFS in different pH 4.5 fluids					
ENM	%	source of in vivo clearance	$t1/2_{in\ vivo}$ (days)	$t1/2_{dissolution}$ (days) calculated from in vivo	PSF	C: MK (phthalate)	D: MG (citrate)	E: MG (HCl)	Muhle	Midander	Shinohara
CeO_2 NM-212	5% cleared per 21d (STIS)	$^{141}CeO_2$ instillation, Molina et al.[72]	140	no contribution of dissolution (>1000)	2001	4371	5998	1252	4567	3610	
TiO_2 NM-105		TiO_2 P25 inhalation, Bermudez et al.[69]	70 to 300 (biphasic)	no contribution of dissolution (>1000)	714	2441	840	2155	149 *	89 *	
SiO_2 NM-200	39% cleared per 21d (STIS)	STIS on SiO_2 untreated, Landsiedel et al.[71]	29	50	31.4	16.6	11.5	15.3	16.9	5.7 *	
$BaSO_4$ NM-220		from $^{131}BaSO_4$ instillation, Konduru et al.[54]	9.6	11.1	6.3	9.1	9.2	7.5	10.5	3.2 *	0.9 *
ZnO NM-111	>93% cleared per 21d (STIS)	STIS, Landsiedel et al., 2011	<5.4	<5.9	0.88	0.31	0.27	1.38	0.24	0.37	

[a]From the study of Bermudez et al.,[69] the results obtained at 2 mg/m^3 (below lung overload) were evaluated. The tested-grade TiO_2 P25 is nearly identical with the physical−chemical properties of the specific batch known as TiO_2 NM-105.[69] All CFS results that deviate by more than a factor of 2 from the derived in vivo halftime are underlined in black and those that are considered as severe conflict are marked by an asterisk.

https://doi.org/10.1021/acs.chemrestox.1c00418
Chem. Res. Toxicol. 2022, 35, 963−980

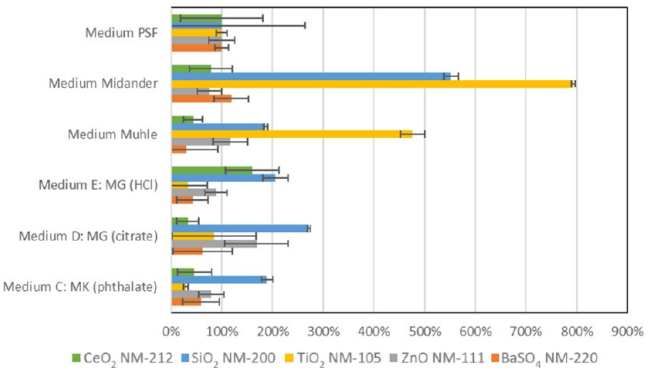

Figure 2. Dissolution rates normalized to the rate in the PSF benchmark medium to clearly visualize the deviation between media. The color code represents the five ENM test materials.

the same ENM in the pH 4.5 PSF medium was published earlier: in short, ZnO particles had disappeared, whereas no change of the particle morphology or size was observed on CeO_2 NM-212 or TiO_2 NM-105; only for $BaSO_4$ NM-220, we had observed Ostwald ripening toward lower radii of curvature, consistent with the in vivo observations.[57,58,60]

For ZnO in any of the five lysosomal pH 4.5 media that had not been investigated in this respect before, no particles were found on TEM grids (empty grids not shown). This is consistent with the 0% remaining mass that is calculated from the quantification of ions (Figure 1).

For the other materials, the median of the TEM constituent particle size distribution and the Feret min and Feret max sizes observed are plotted in Figure 4. The given values for particle sizes always refer to primary particles. The error bars are set to 10% considering a systematic calibration error of the TEM of ~5% and systematic errors of the particle size analysis of another 5% resulting from segmentation errors of the particles. Additional errors, resulting from, for example, the automated image analysis, were not estimated and might be larger than the 5% segmentation error. Min and max values are more affected by the statistical fluctuation than the median. Standard deviations of the mean value are usually rather large (25−50% of the mean value) indicating significant statistical errors of min, max, and median. The number of particles analyzed for each material and medium was between 150 and 1500. An ANOVA variance analysis of all three size descriptors resulted in significant differences between the size after incubation in different media as well as between any medium and the pristine sample for TiO_2, CeO_2, and $BaSO_4$. For these materials, the smallest particles that were quantitatively pelletted onto the grid (see Experimental Testing) were below the detected min value, which is hence not limited by the sample preparation. For SiO_2, only the difference between the pristine material and samples in media is significant but not the differences between incubation in different media. The detected min value of SiO_2 was close to the calculated diameter of the smallest dispersed particle that would have been quantitatively pelletted onto the TEM grid (see Experimental Testing). Although we mostly detect large SiO_2 agglomerates, one cannot exclude the fact that dispersed SiO_2 particles below 9 nm were underrepresented by the TEM analysis after dissolution.

Representative TEM images of TiO_2 and $BaSO_4$ are given in Figures 5 and 6. TEM images of CeO_2 and SiO_2 are shown in the Supporting Information (Figures SI_2 and SI_3). The morphology of the samples was assessed by inspection of the images. No qualitative differences are visible for TiO_2 and CeO_2. Particles seem to be more agglomerated for some media (e.g., TiO_2—Media C and E). This is most likely an effect of remaining salts from the media, which were deposited between the particles of the agglomerates, but the image evaluation reported sizes of primary particles within agglomerates. The pristine $BaSO_4$ morphology changed after exposure to media, promoting more round shaped particles with reduced radii of curvature, consistent with earlier findings on PSF. Silica showed a more pronounced morphology change (Figure SI_3). Particles partly merged and formed a sponge-like network. This aggregation phenomenon was already observed in previous studies due to the reduced pH values and high salinity in medium composition.[64−68] Choi and Kim observed by TEM, after 7-day exposure, that the SiO_2 ENM morphology partially changed, forming a sponge-like structure.[64] The parallel GRACIOUS (Grouping, Read-Across, CharacterIzation, and classificatiOn framework for regUlatory risk assessment of manufactured nanomaterials and Safer design of nano-enabled products) project adds evidence on the transformation of a family of silica NFs in both lysosomal pH 4.5 and extracellular pH 7.4 fluids.[60] In short, colloidal silica NFs transformed into a gel-like morphology especially in the pH 7.4 medium, and Al-doping modulated the dissolution and transformation more than the pristine aspect ratio. This was not as prominently observed

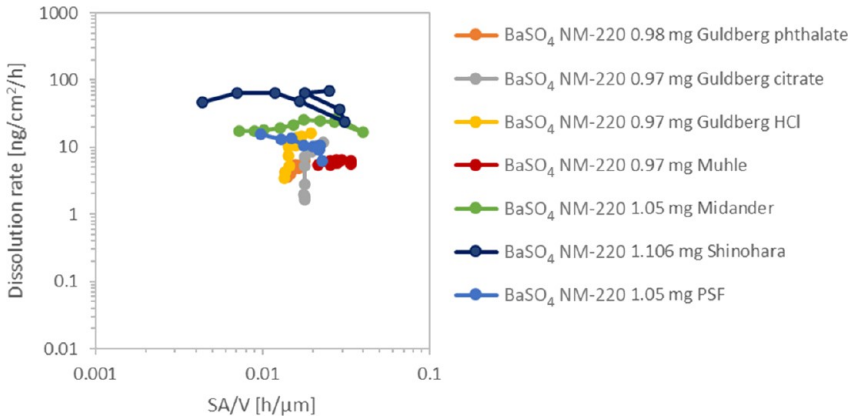

Figure 3. Detailed trajectory of the dissolution rates of $BaSO_4$ NM-220 during dissolution testing. Each trajectory starts on the right and then moves to the left due to the reduction of the total surface area.

https://doi.org/10.1021/acs.chemrestox.1c00418
Chem. Res. Toxicol. 2022, 35, 963−980

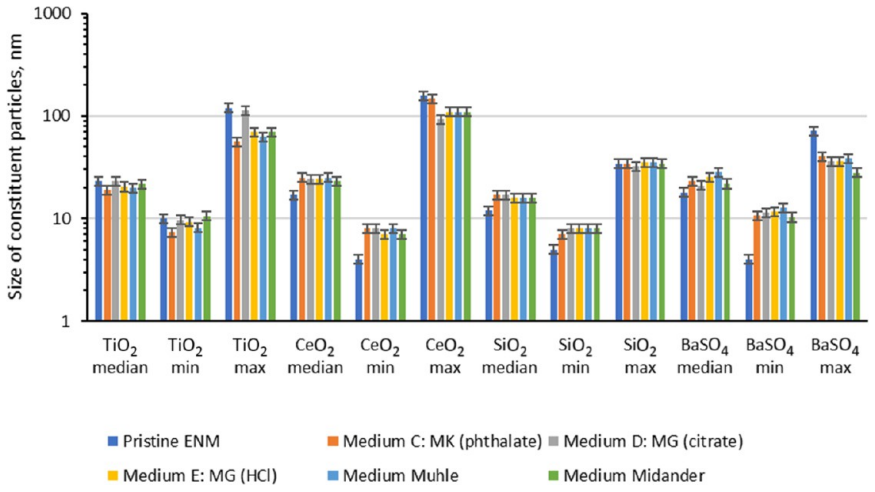

Figure 4. Summary of TEM evaluation of up to 1500 particles, represented by the descriptors of D50 number median and supported by the statistics of min and max diameters. The error bars reflect the known systematic error of the TEM evaluation. Table SI_3 includes further information.

on SiO_2 NM-200.[60] Due to the different production processes resulting in different surface chemistries, the behavior of colloidal silica may differ from that of precipitated or pyrolytic silica.

DISCUSSION

Validity of pH 4.5 Lysosomal Simulant Fluids for ENM Dissolution. The validity of pH 4.5 lysosomal simulant fluids can be assessed by the accuracy of the prediction of the contribution of dissolution to clearance from the lungs. This criterion then also implies the correct ranking of the dissolution rates of different ENM. For the rat, lung retention halftimes ($t1/2$) for "poorly soluble low-toxicity" particles are about 70 days and, by definition, reflect mechanical, macrophage-mediated clearance, generally following first-order kinetics.[3] Knowing that the total lung particle clearance reflects the sum of mechanical and dissolution clearance, we derived from published inhalation studies the contribution of dissolution to the clearance of the materials that were studied here (Table 3).

For both CeO_2 NM-212 and TiO_2 NM-105, the in vivo evidence suggests no contribution of dissolution (Table 3). The measured halftimes in the PSF medium range above 1000 days and can thus be considered as matching with the in vivo evidence. In contrast, the Muhle and Midander media result in considerable dissolution with halftimes of 149 days and 89 days, respectively. This extent of dissolution would have been clearly observable during the 90-day inhalation studies but was not (Table 3).[69] The Muhle medium and Midander medium are thus in conflict with the in vivo findings on the TiO_2 material.

SiO_2 NM-200 is cleared by a combination of physical clearance and dissolution with a derived dissolution halftime of 50 days. This value is adequately matched by the CFS measurement with the PSF fluid at a halftime of 41.3 days, and also the C:MK (phthalate), E:MG (HCl), and Muhle media are close with values around 29 days. Only the measurement with the Midander medium, with a halftime of 4.8 days, is in conflict with the in vivo findings on the SiO_2 NM-200 material. With regard specifically to $BaSO_4$ pulmonary clearance and transformation, Konduru and colleagues reported that intratracheally instilled ^{131}Ba-labeled $BaSO_4$ NM-220 exhibited a lung retention halftime of 9.6 days in rats and that ^{131}Ba was incorporated into the bones, suggesting nanoparticle dissolution with a halftime of 11.1 days.[54] The dissolution halftime measured with the PSF fluid in the CFS correctly finds significant dissolution but is somewhat too low at 5.8 days, but likely within the uncertainty of the method. In the $BaSO_4$ case, $t1/2$ values obtained in other media such as C:MK (phthalate), D:MG (citrate), and Muhle result in values that are closer to the in vivo derivation. However, the Midander and Shinohara media result in halftimes as low as 0.9 days and are thus in conflict with the in vivo findings on the $BaSO_4$ NM-220 material.

The biokinetics of ZnO NM-111 in the tested inhalation study design allows to derive only an upper limit on the in vivo dissolution halftime of <5.9 days (Table 3). CFS measurements with all media agree closely on a dissolution halftime of 0.6 to 0.7 days. This value is in accord with the in vivo findings for this material. The good agreement on fast dissolution can be attributed to the steep pH dependence of ZnO solubility,[60] where all other factors seem to be less important.

In Table 3, all CFS results that deviate by more than a factor of 2 from the derived in vivo halftime are considered as conflict and are underlined in black. This criterion is debatable with regard to the metrological significance and with regard to the biological relevance: the factor of 2 supports the reproducibility of the CFS method. We independently assessed the reproducibility of the CFS method on TiO_2 NM-104 and ZnO NM-110 (data not shown, NanoHarmony and PATROLS projects) and found about 40% reproducibility for both materials; this value is in the range of 67% found in earlier interlab comparisons on the CFS method,[61] and thus a factor of 2 can be considered as the metrological limit of significance. Depending on the toxicity of the material studied, differences of a factor of 2 may already impact the hazard assessment; the ECETOC (European Centre for Ecotoxicology and Toxicology Of Chemicals) NanoApp recommended up to a factor of 3 difference in dissolution rates as acceptable for joint hazard assessment.[73,74]

By removing all media that result in at least one conflict with in vivo findings, we conclude that three lysosomal simulant media are consistent with each other and with in vivo clearance:

- modified Kanapilly (denoted as Guldberg_phthalate, medium C: MK)
- phagolysosomal simulant fluid (denoted as PSF)
- modified Gamble's (denoted as Guldberg_HCl, medium E: MG)

https://doi.org/10.1021/acs.chemrestox.1c00418
Chem. Res. Toxicol. 2022, 35, 963−980

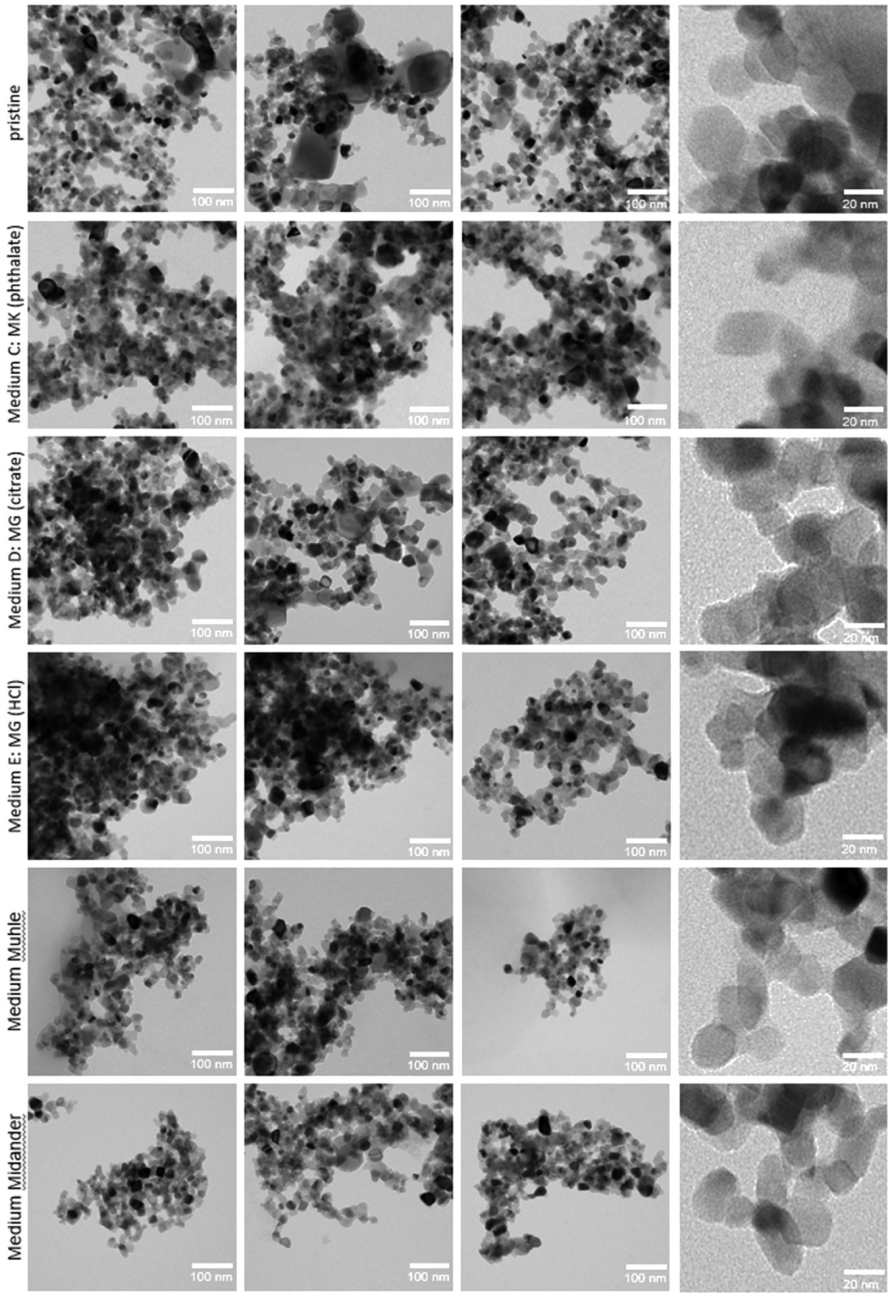

Figure 5. TEM analysis of pristine TiO_2 NM-105 and after 7 days of dissolution testing in different pH 4.5 test media. For each medium, three spots on the TEM grid were imaged and evaluated.

These media predict the quick dissolution of ZnO NM-111, the relatively fast intermediate dissolution of SiO_2 NM-200, and the very slow dissolution of TiO_2 NM-105. It is the remarkable robustness of the CFS method that despite the variation of the absolute rates by a factor of 3700 (k = 0.02 to 74 ng/cm^2/h), the valid media are consistent with each other within a factor of 2 for all materials. The differences between the CFS results with the three media are thus comparable to the CFS method reproducibility itself.

On SiO_2 NM-200 specifically, the Midander medium results in a dissolution halftime that deviates nearly 10-fold from the in vivo findings. This must be considered as severe conflict. Only the PSF medium for SiO_2 NM-200 results in a dissolution halftime that remains within a factor of 2 of the in vivo finding; however, one must consider that the in vivo study used colloidal amorphous silica ("SiO_2 untreated"),[71] whereas NM-200 is precipitated amorphous silica.[75] Despite the near-identical specific surface area of around 200 m^2/g for both materials, differences, for example, in the silanol groups, may induce different biological interactions.[76,77] One also notes that not all nanoparticles end up in lysosomes.[78,79] Others, including silica, are less soluble under the acidic lysosomal conditions than under the neutral conditions of the epithelial lining fluid.[80] Hence, we did not consider any specific medium as not valid only on the basis of SiO_2 results.

Based on a false prediction of partial dissolution of TiO_2 NM-105 (which in vivo is very slow), and on the false prediction of quick dissolution of $BaSO_4$ NM-220 (which in vivo is only partial), we cannot recommend the following media as simulant fluids for lysosomal fluids in CFS testing:

https://doi.org/10.1021/acs.chemrestox.1c00418
Chem. Res. Toxicol. 2022, 35, 963−980

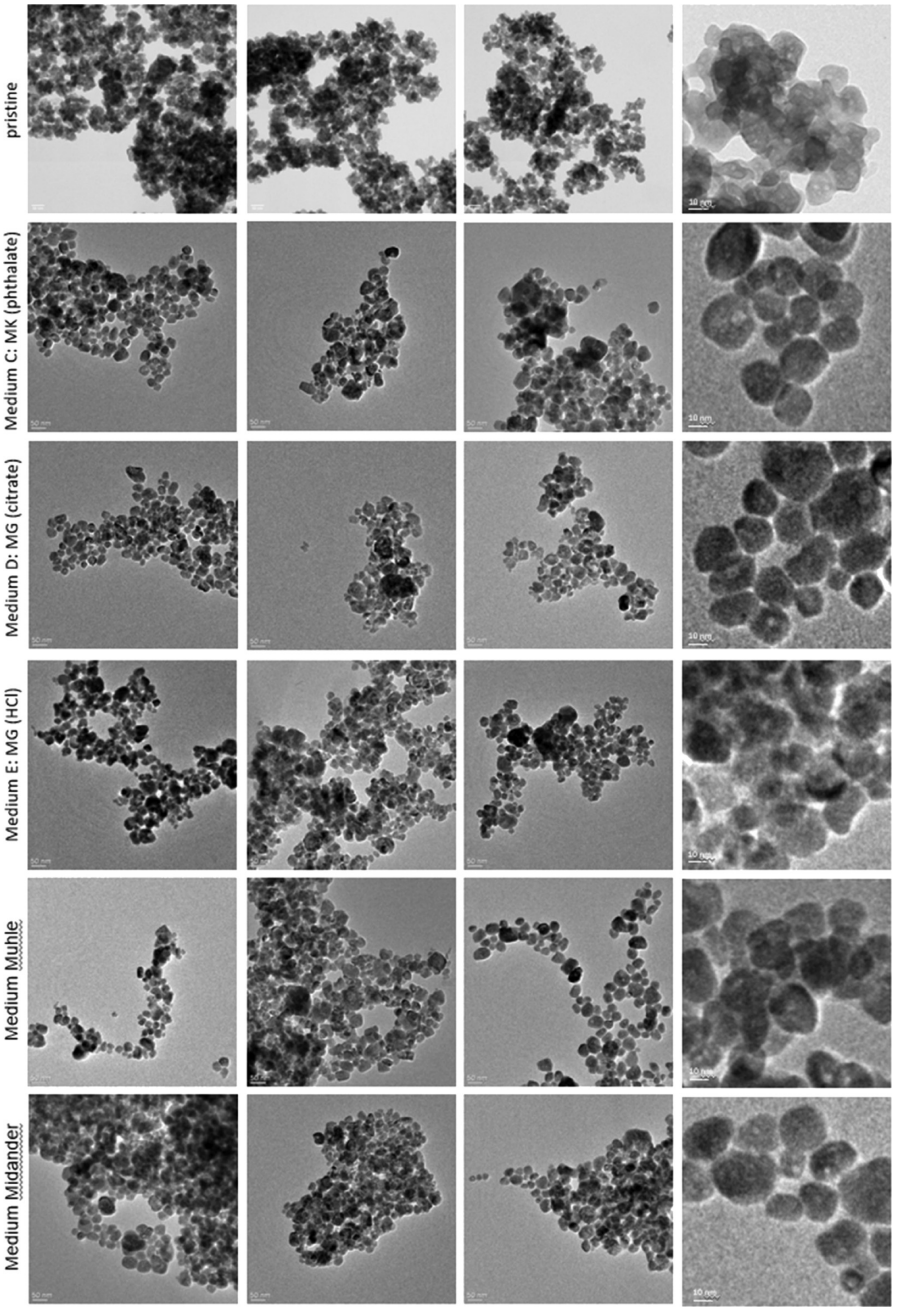

Figure 6. TEM analysis of pristine $BaSO_4$ NM-220 and after 7 days of dissolution testing in different pH 4.5 test media. For each medium, three spots on the TEM grid were imaged and evaluated.

- Medium "Midander" because of three conflicts on TiO_2, SiO_2, and $BaSO_4$
- Medium "Muhle" because of a conflict on TiO_2
- Medium "Shinohara" because of a conflict on $BaSO_4$.

One notes that all the "invalid" media use citric acid at concentrations above 5 g/L (up to 28 g/L). In contrast, the valid media use either a mix of organic acids (with the total concentration below 0.5 g/L, thereof citric acid below 0.15 g/L) or another organic acid (KH phthalate) at 4 g/L. For several ENM, including ZnO, $BaSO_4$, and CeO_2, all these differences induce only minor modulation of the dissolution rates. We had tested earlier on $BaSO_4$ that pH and temperature are decisive for the dissolution rate but not the specific organic acid that mimics the presence of enzymes.[58] Only for TiO_2 and SiO_2, the interaction with specific organic acids is highly sensitive, probably due to sequestration of the ions or direct interaction with the surfaces,[81] and can lead to wrong predictions when compared to the in vivo behavior. This sensitivity to the simulant composition (and the attribution to ion sequestration) is well known from the dissolution of glass fibers.[82]

The new results can be compared against earlier comparison between abiotic, in vitro, and in vivo dissolution rates (Table 4): Stefaniak et al. compared 200 nm beryllium oxide dissolution in PSF (in a static system) to dissolution in mouse J774A.1 cells and further assessed how the ionic composition of the extraction fluid, buffer strength, and the presence of an antifungal agent affected beryllium dissolution.[22] Beryllium dissolution in PSF did not differ from dissolution in the J774A.1 cells or from dissolution in the pH 4.5 Baron and Ahmed solution (Table 2 of

https://doi.org/10.1021/acs.chemrestox.1c00418
Chem. Res. Toxicol. 2022, 35, 963−980

Table 4. Biodissolution Studies Assessing Fibers or Nanomaterials in pH 4.5 Extraction Fluids

study	pH 4.5 extraction fluid	test materials	comparison of abiotic dissolution rate to in vitro cellular and/or in vivo effects
Guldberg et al.[17]	Five different fluids (Table 2)	MMVF21, MMVF22, and MMVF34	apart from the fluid containing citric acid, accurate prediction of in vivo pathogenicity and lung clearance rates as reported in IARC[89] (Table 65)
Stefaniak et al.[22]	PSF	beryllium oxide	accurate prediction of in vitro dissolution in mouse J774A.1 cells and in vivo dissolution in dogs (acute inhalation exposure)
Koltermann-Jülly et al.[57] with addendum (2019)		different (nano-)forms of $BaSO_4$, CeO_2, Cu-phthalocyanine/CuO, Fe_2O_3, SiO_2, $SrCO_3$, TiO_2, and ZnO	good correlation with in vitro dissolution in cultured rat NR8383 AMs and with pulmonary clearance in rat STISs
Keller et al.[58]		nano- and nonnano forms of $BaSO_4$, TiO_2, kaolin, and bentonite and nanoforms of ZnO w/ and w/o coating	also method parameters such as flow rate are critical: with PSF, all benchmark materials were correctly predicted in a specific valid range of SA/V
Keller et al.[59]		$BaSO_4$	good correlation with in vivo pulmonary clearance in rats and with in vivo transformation (Ostwald ripening) in rats
Jeong et al.[84]	as published by Stopford et al.[43]	CuO NPs and indium oxide NPs	consistent with pulmonary effects observed in rats upon oral pharyngeal aspiration
Adamcakova-Dodd et al.[85]		ZnO NPs	good correlation with dissolution in 2- and 13-week mouse inhalation toxicity studies
Latvala et al.[86]	as published by Midander et al.[21]	Nanosized and micron-sized Ni-containing particles	insufficient correlation—dissolution in the cell culture was slower than in the abiotic system
Shinohara et al.[42]	as published by Shinohara et al.[42]	nano- and micron-sized NiO	Good correlation with pulmonary clearance in the rat intratracheal instillation studies

our briefing). A buffer concentration of 0.01 M KH phthalate did not appear adequate to maintain the pH stable over the 10-day evaluation period. Therefore, it was increased to 0.02 M KH phthalate, which yielded pH stability without altering the dissolution rates. Addition of the antifungal agent did not affect beryllium dissolution in PSF. Stefaniak et al.[22] concluded that PSF is an appropriate extraction fluid to assess beryllium dissolution in a static test system.

ISO/TR 19057[15] also discusses the findings from the study by Stefaniak et al.,[22] further considering the in vivo dissolution data of the same 200 nm beryllium oxide obtained in a dog acute inhalation toxicity study.[83] As summarized in ISO/TR 19057,[15] the dissolution rate constant in PSF (1.2×10^{-8} g/cm^2/d) was within twofold of the rate constant determined in J774A.1 cells (2.3×10^{-8} g/cm^2/d) and showed good agreement to the rate constant determined in the Beagles (0.7×10^{-8} g/cm^2/d).

ISO/TR 19057[15] further discussed a study on the dissolution behavior of indium oxide NPs and CuO NPs under acidic conditions.[84] Jeong et al. reported the use of a "pH 5.5" artificial lysosomal fluid (ALF; incubation for 1 and 28 days) and referred to the study by Stopford et al.[43] for details on the composition of this fluid. In parallel, Jeong et al.[84] recorded particle toxicity in rats upon oral pharyngeal aspiration (under anesthesia) up to 28 days postexposure. As summarized in ISO/TR 19057,[15] CuO NPs dissolved very rapidly in ALF (97.3% on day 1 and 100% on day 28). In vivo, CuO NPs elicited severe neutrophilic inflammation on day 1 that completely resolved by day 14. Indium oxide NPs dissolved much more slowly, but progressively, in ALF (0.6% on day 1 and 5.5% on day 28); consistently, the in vivo results showed progressive neutrophilic inflammation from day 1 to day 28 and severe pulmonary alveolar proteinosis on day 28.[15]

ISO/TR 19057[15] concludes that while the presented studies do not validate abiotic dissolution tests, they do suggest that these tests are a starting point to produce biologically relevant data that aid risk assessment.

Koltermann-Jülly et al. tested altogether 24 different (nano-)forms of $BaSO_4$, CeO_2, CuO/Cu-phthalocyanine, Fe_2O_3, SiO_2, $SrCO_3$, TiO_2, and ZnO using an abiotic flow-through method with the PSF medium and compared these data with the in vitro dissolution behavior in NR8383 rat AM cell cultures (F12-K medium supplemented with 5% fetal calf serum (FCS), 48 h incubation) and lung clearance rates in rat short-term inhalation studies (STISs, 5-day exposure, 6 h/day).[57] Overall, the findings from the study by Koltermann-Jülly et al. showed that the abiotic dissolution rates were consistent with the effects observed in vivo in the rat STIS and with the in vitro effects recorded in cultured NR8383 AMs. Furthermore, dissolution properties were generally similar between different (nano-)forms of the same chemical substance, whereas they differed by more than 1000-fold between different chemical substances. Between different (nano-)forms of the same chemical substance, variations in the dissolution behavior could be explained by differences in production routes, surface area, or coating. By contrast, effects of shape or size on dissolution behavior were limited.[57]

Yokel et al. compared the dissolution of 4 nm CeO_2 in pH 4.5 simulant fluids containing organic acids (alternatively acetic, adipic, citric, glutaric, DL-3-hydroxybutyric, lactic, DL-malic, pimelic, and succinic acids).[50] Its concentration of 110 mM corresponds, for citric acid, to 21 g/L and is thus comparable to the Midander medium or Shinohara medium. Yokel et al. found up to fourfold difference of dissolution halftimes (between 33

https://doi.org/10.1021/acs.chemrestox.1c00418
Chem. Res. Toxicol. 2022, 35, 963−980

and 126 days) induced by the different acids. They attributed the relatively fast dissolution to the enrichment of less stable Ce^{3+} on the surface of their very small CeO_2, which also differed by its hydrothermal synthesis route without calcination from the precipitated NM-212. It can thus occur that less stable nanoforms of CeO_2 become more sensitive to the choice of the simulant medium.

Adamcakova-Dodd et al. tested 3.5 mg/m^3 ZnO NPs (primary particle size: 10 nm) in 2- or 13-week mouse inhalation studies (4 h exposure/day).[85] Zn^{2+} concentrations in the bronchoalveolar lavage fluid (BALF) were increased immediately after exposure but returned to baseline levels 3 weeks postexposure. Furthermore, BALF macrophages were increased and interleukin-12(p40) and macrophage inflammatory protein-1α moderately increased. In abiotic dissolution studies, the ZnO NPs readily dissolved at pH 4.5 but formed aggregates and precipitates at pH 7.4. These results support the findings for ZnO NPs recorded by Koltermann-Jülly et al.[57]

Latvala et al. assessed two nanosized and two micron-sized Ni-containing particles in a static dissolution system.[86] After 24 h, the released amount of Ni was notably higher in ALF (e.g., 80−100 wt % for metallic Ni) than in Dulbecco's modified eagle medium supplemented with 10% FCS (DMEM + FCS) (approx. 1−3 weight% for all particles). Furthermore, human A549 cells cultured in DMEM + FCS were exposed to the Ni-containing particles. All test materials were taken up by the cells within 4 h and mostly remained in the cells for 24 h postincubation. Latvala et al.[86] concluded that the high dissolution in ALF did not reflect intracellular particle dissolution (notably, it remains to be determined why dissolution in a biologically more complex system was slower than in the abiotic system).

By contrast, Shinohara et al. recorded that nano- and micron-sized NiO that dissolve rapidly in ALF are easily cleared from the rat lungs (upon intratracheal instillation).[42] Only nanosized NiO elicited pulmonary clearance overload. Shinohara et al.[42] concluded that these findings suggest that the clearance mechanisms do not involve AM migration to the end of bronchi but rather dissolution in AM lysosomes.

Several issues remain open. For example, more realistic, complex fluids with enzymes[87,88] may promote incongruent dissolution and reprecipitation phenomena of multicomponent (nano)materials by selective interaction with individual components. Chemical speciation analysis by EDX, XRD, or SAD will become required. Furthermore, no data are known to us reporting the in vivo clearance of the same particle with and without coating, but one expects that surface treatments or coatings can modulate the dissolution behavior. Such a modulation was observed on coated nanomaterials.[54,59] Here, both coated and uncoated materials were selected because of the existence of suitable in vivo clearance data.

Supporting Evidence from Studies of Mineral Fibers. Guldberg et al. comparatively assessed the dissolution rates for five man-made vitreous fibers (MMVF) obtained in fluids B, C, and D.[17] For five different MMVFs, representing in vivo pulmonary clearance halftimes from days to years,[90] the dissolution rate in the citric acid-containing fluid D was much higher than in fluids B and C; for the biosoluble MMVF34, the rate was even 200-fold higher (i.e., 13,000 ng/cm^2/h vs 700 and 600 ng/cm^2/h in fluids B and C, respectively). The authors noted correctly that this extremely high dissolution rate does not match with the in vivo lung clearance rate of MMVF34.[91] By comparison, the MMVF34 dissolution rates in fluids B and C were widely identical, just as the same dissolution rate was recorded for MMVF22 in either fluid B or C, but for another composition, named MMVF21, the dissolution rate in fluid B was higher than in fluid C (60 vs 22 ng/cm^2/h). Thereby, both values correctly predicted the long in vivo half-life of MMVF21, whereas the high MMVF21 dissolution rate in citrate-containing fluid D (220 ng/cm^2/h) incorrectly predicted clearance within weeks, corresponding to a wrong prediction of nonpathogenicity. In summary, the pH 4.5 extraction fluids assessed by Guldberg et al. generally appeared suitable for dissolution rate testing of stone and slag wool fibers, except for the fluid D ("MG (citrate)").

More recently, but on the identical media, Sauer et al. have experimentally demonstrated how the fluid composition and binder affect the abiotic dissolution of a representative stone wool MMVF.[19] Several of the same fluids that we tested on ENM in the present study had a critical difference on MMVF in their ability to modulate the formation of Si-rich gels on the fiber surfaces. Removing the binder accelerated the average dissolution rate by +104% (max +273%) across the fluids, and this quantitative change was concomitant with a qualitative change of secondary structures, such as leaching pits, gels, collapsed bubbles, and crystalline deposits.[92] To enhance the reliability and robustness of abiotic predictions of biodurability, Sauer et al. recommended replacing the critically influential citric acid in pH 4.5 fluids by other organic acids. Also they recommended that future studies should consider structural transformations of the fibers, including changes in fiber length, fiber composition, and reprecipitation of gel layers.[19] However, the increased sensitivity of MMVF to the specific composition of the simulant medium originates also from its multicomponent composition containing Si, Al, Fe, Ca, Na, Fe, Ti, etc. as a mixed metal oxide. Incongruent dissolution and leaching of the different metals can lead to preferential sequestration or reprecipitation, depending on the binding partners present in the organic binder or in the simulant medium. Such a complex behavior may not be expected for monoconstituent ENM as studied here and discussed in the next section.

Impact of Lysosomal pH 4.5 Simulant Fluids on ENM Transformation. By using TEM, we explored the extent to which different media induce size shrinkage or other relevant transformations of the ENM test materials. Unexpectedly, from image analysis, we observed rather little difference in particle sizes and morphologies after testing in the different media, even for those that deviated in the dissolution kinetics. Ti and Si ions, which showed the highest sensitivity toward sequestration by specific organic acids, could have shown a tendency to reprecipitate on existing particles, forming larger crystals via a saturation (Oswald ripening) mechanism. Indeed, the solubility limit is relevant for TiO_2 in the CFS because by variation of the volume flow rate $\dot{V}$ in the CFS, we had found a linear $1/\dot{V}$ impact on the apparent dissolution rate k of TiO_2 NM-105.[59] This is a telltale effect of saturation according to the modeling of CFS.[59] However, the very low fraction of the initial TiO_2 mass that ever becomes dissolved during the experiment—less than 0.5% for most media and up to 3% for the invalid media—would not even suffice to induce detectable morphological changes within the reproducibility and accuracy of TEM measurements before and after dissolution. Indeed, no transformation on TiO_2 NM-105 was observed (Figures 4 and 5) nor on CeO_2 NM-212 (Figures 4 and Figure SI_2).

A higher magnification would improve the precision in particle size determination for in situ studies on one and the

https://doi.org/10.1021/acs.chemrestox.1c00418
Chem. Res. Toxicol. 2022, 35, 963−980

same particle. However, the TEM analysis in CFS is an ex situ ensemble strategy where we compare statistical measures and not single particles. As the released mass scales with the third power of diameter, it is expected that small releases as measured for, for example, TiO_2 are not detectable by particle size analysis.

Transformation impacted SiO_2 samples that showed the formation of partially sintered or gelled SiO_2 structures with a sponge-like morphology (Figures 4 and Figure SI_3) and on $BaSO_4$ particles with the formation of a rounded morphology (Figures 4 and 6). Ostwald ripening of $BaSO_4$ was also observed on the lung specimen in vivo.[58] Due to the Ostwald ripening, the polydispersity of the $BaSO_4$ particle size reduces. In accordance with the relatively low modulation of $BaSO_4$ dissolution rates by different pH 4.5 simulant fluids, also the TEM investigations showed the same structural transformation of $BaSO_4$ to more rounded shapes in any of the pH 4.5 media, pointing to pH and temperature, not the organic acids, as a primary trigger of Ostwald ripening.

As an interim conclusion, investigation of the size changes and transformation after CFS dissolution testing does not seem to be a promising descriptor of the ENM dissolution in physiological media. Yet, electron microscopy characterization is still anticipated to be relevant for improved understanding of mechanisms and morphological changes in long-term testing. Especially advanced single-particle studies by in situ high-resolution TEM may contribute to mechanistic understanding but are not adequate for regulatory purposes.

CONCLUSIONS

A variety of different pH 4.5 lysosomal simulant fluids have been used in abiotic dissolution studies. Differences in chemical compositions of simulant fluids are often minimal and generally not justified. The influence of individual components of pH 4.5 extraction fluids on dissolution rates and the impact of the addition of further organic compounds, such as amino acids and proteins, are not sufficiently understood to justify the selection of any single simulant fluid as being the most suitable in reflecting the acidic environment of AM lysosomes.

Here we found that three out of the eight lysosomal simulant media are consistent with each other and with in vivo clearance:

- modified Kanapilly (denoted as Guldberg_phthalate, medium C: MK)
- phagolysosomal simulant fluid (denoted as PSF)
- modified Gamble's (denoted as Guldberg_HCl, medium E: MG)

Using these three media, the quick dissolution of ZnO NM-111, intermediate (partial) dissolution of SiO_2 NM-200 and $BaSO_4$ NM-220, and the very slow dissolution of TiO_2 NM-105 and CeO_2 NM-212 are observed in concordance with the results on pulmonary clearance from in vivo studies. We also identified several media as invalid based on conflicts with the in vivo findings, most notably an incorrect prediction of TiO_2 dissolution under pulmonary conditions. All the invalid media showing incorrectly fast dissolution rates for SiO_2 and TiO_2 materials use citric acid at concentrations above 5 g/L (up to 28 g/L) and could lead to wrong predictions of the in vivo behavior. In contrast, the valid media use either a mix of organic acids (with the total concentration below 0.5 g/L, thereof citric acid below 0.15 g/L) or another organic acid (KH phthalate) at 4 g/L. For ZnO, $BaSO_4$, and CeO_2, there was only minor modulation of the dissolution rates when using the "invalid" media because the pH is the dominant parameter for these materials.

Size and morphology analyses by electron microscopy might be a relevant tool to assess the mechanisms of dissolution as well as potential transformation and respeciation phenomena, while morphology and size changes are best assessed after relatively long exposures. In the present selection of ENM tested in the CFS, the only small changes were observed after dissolution of SiO_2 and $BaSO_4$, resulting in sponge-like gelled aggregates and rounder structures, respectively, which may be linked to saturation in media during testing. More complex transformations can be expected for multicomponent (nano)-materials due to incongruent dissolution and potential reprecipitation. In general, however, the TEM investigations were not able to quantify dissolution and are thus not recommended to replace ion quantification as the main analytical tool.

In summary, we recommend the standardization of ENM dissolution testing by one of the three valid lysosomal simulant fluids with determination of the dissolution rate and halftime by the quantification of ions. This recommendation was established based on the CFS but may be relevant as well for static (batch) solubility testing. We recommend such standardization especially for the ongoing OECD project on "Determination of solubility and dissolution rate of nanomaterials in water and relevant synthetic biological media" and the interlaboratory comparison that are being planned in this frame. With a choice of three valid media, the future user still has options, for example, in the case of interferences of specific components with the detection of the target analyte. We also conclude that representative test materials such as the specific batches of ZnO, $BaSO_4$, and TiO_2, which are available from the JRC Repository, are highly useful to demonstrate the proficiency in dissolution testing of unknown ENM.

ASSOCIATED CONTENT

Supporting Information

The Supporting Information is available free of charge at https://pubs.acs.org/doi/10.1021/acs.chemrestox.1c00418.

Details on the literature review, simulant media composition, and TEM images of SiO_2 and CeO_2 (PDF)

AUTHOR INFORMATION

Corresponding Author

Wendel Wohlleben − *Department of Material Physics and Analytics and Department of Experimental Toxicology and Ecology, BASF SE, Ludwigshafen 67056, Germany;* orcid.org/0000-0003-2094-3260; Email: wendel.wohlleben@basf.com

Authors

Ilaria Zanoni − *CNR-ISTEC-National Research Council of Italy, Institute of Science and Technology for Ceramics, Faenza 48018, Italy*

Johannes G. Keller − *Department of Material Physics and Analytics and Department of Experimental Toxicology and Ecology, BASF SE, Ludwigshafen 67056, Germany*

Ursula G. Sauer − *Scientific Consultancy-Animal Welfare, Neubiberg 85579, Germany*

Philipp Müller − *Department of Material Physics and Analytics, BASF SE, Ludwigshafen 67056, Germany*

Lan Ma-Hock − *Department of Experimental Toxicology and Ecology, BASF SE, Ludwigshafen 67056, Germany*

https://doi.org/10.1021/acs.chemrestox.1c00418
Chem. Res. Toxicol. 2022, 35, 963−980

Keld A. Jensen − *National Research Centre for Work Environment (NRCWE), Copenhagen 2100, Denmark*
Anna Luisa Costa − *CNR-ISTEC-National Research Council of Italy, Institute of Science and Technology for Ceramics, Faenza 48018, Italy*

Complete contact information is available at: https://pubs.acs.org/10.1021/acs.chemrestox.1c00418

Notes

The authors declare the following competing financial interest(s): JGK, PM, LMH, WW are employees of BASF SE, a company producing nanomaterials.

■ ACKNOWLEDGMENTS

The authors would like to acknowledge that this research has received funding from the European Union's Horizon 2020 research and innovation program for the PATROLS project, under Grant Agreement No.760813. K.A.J. would also like to acknowledge funding received from the GOV4NANO project under Grant Agreement 814401.

■ REFERENCES

(1) Christensen, V. R.; Lund Jensen, S.; Guldberg, M.; Kamstrup, O. Effect of Chemical Composition of Man-Made Vitreous Fibers on the Rate of Dissolution in Vitro at Different PHs. *Environ. Health Perspect.* **1994**, *102*, 83−86.
(2) Kastury, F.; Smith, E.; Juhasz, A. L. A Critical Review of Approaches and Limitations of Inhalation Bioavailability and Bioaccessibility of Metal(Loid)s from Ambient Particulate Matter or Dust. *Sci. Total Environ.* **2017**, *574*, 1054−1074.
(3) Oberdörster, G.; Kuhlbusch, T. A. J. In Vivo Effects: Methodologies and Biokinetics of Inhaled Nanomaterials. *NanoImpact* **2018**, *10*, 38−60.
(4) Utembe, W.; Potgieter, K.; Stefaniak, A. B.; Gulumian, M. Dissolution and Biodurability: Important Parameters Needed for Risk Assessment of Nanomaterials. *Part. Fibre Toxicol.* **2015**, *12*, 11.
(5) Guldberg, M.; Krois, W.; Sebastian, K.; Christensen, V. R. Method for Determining In-Vitro Dissolution Rates of Manmade Vitreous Fibres. *Glass Sci. Technol.* **1995**, *68*, 181−187.
(6) Innes, E.; Yiu, H. H. P.; McLean, P.; Brown, W.; Boyles, M. Simulated Biological Fluids − a Systematic Review of Their Biological Relevance and Use in Relation to Inhalation Toxicology of Particles and Fibres. *Crit. Rev. Toxicol.* **2021**, 1−32.
(7) McGillicuddy, E.; Murray, I.; Kavanagh, S.; Morrison, L.; Fogarty, A.; Cormican, M.; Dockery, P.; Prendergast, M.; Rowan, N.; Morris, D. Silver Nanoparticles in the Environment: Sources, Detection and Ecotoxicology. *Sci. Total Environ.* **2017**, *575*, 231−246.
(8) Hoet, P. H. M.; Brüske-Hohlfeld, I.; Salata, O. V. Nanoparticles − Known and Unknown Health Risks. *J. Nanobiotechnol.* **2004**, *2*, 12.
(9) Franz, T. J. Percutaneous Absorption. On the Relevance of in Vitro Data. *J. Invest. Dermatol.* **1975**, *64*, 190−195.
(10) Wohlleben, W.; Waindok, H.; Daumann, B.; Werle, K.; Drum, M.; Egenolf, H. Composition, Respirable Fraction and Dissolution Rate of 24 Stone Wool MMVF with Their Binder. *Part. Fibre Toxicol.* **2017**, *14*, 1−16.
(11) Bauer, J. F.; Law, B. D.; Hesterberg, T. W. Dual PH Durability Studies of Man-Made Vitreous Fiber (MMVF). *Environ. Health Perspect.* **1994**, *102*, 61−65.
(12) Sebastian, K.; Fellman, J.; Potter, R. M.; Bauer, J.; Searl, A.; de Meringo, A.; Maquin, B.; de Reydellet, A.; Jubb, G.; Moore, M.; Preininger, R.; Zoitos, B.; Boymel, P.; Steenberg, T.; Madsen, A. L.; Guldberg, M. EURIMA Test Guideline: In-Vitro Acellular Dissolution of Man-Made Vitreous Silicate Fibres. *Glass Sci. Technol.* **2002**, *75*, 263−270.
(13) Okhrimenko, D. V.; Bøtner, J. A.; Riis, H. K.; Ceccato, M.; Foss, M.; Solvang, M. The Dissolution of Stone Wool Fibers with Sugar-Based Binder and Oil in Different Synthetic Lung Fluids. *Toxicol. In Vitro* **2022**, *78*, No. 105270.
(14) Boisa, N.; Elom, N.; Dean, J. R.; Deary, M. E.; Bird, G.; Entwistle, J. A. Development and Application of an Inhalation Bioaccessibility Method (IBM) for Lead in the PM10 Size Fraction of Soil. *Environ. Int.* **2014**, *70*, 132−142.
(15) *ISO/TR 19057:2017 Nanotechnologies — Use and Application of Acellular in Vitro Tests and Methodologies to Assess Nanomaterial Biodurability*, 2017.
(16) OECD. *Organisation for Economic Cooperation and Development Guidance Document No. 29 on Transformation / Dissolution of Metals and Metal Compounds in Aqueous Media*; Paris, France, 2001.
(17) Guldberg, M.; Christensen, V. R.; Perander, M.; Zoitos, B.; Koenig, A. R.; Sebastian, K. Measurement of In-Vitro Fibre Dissolution Rate at Acidic PH. *Ann. Occup. Hyg.* **1998**, *42*, 233−243.
(18) Rozalen, M.; Ramos, M. E.; Huertas, F. J.; Fiore, S.; Gervilla, F. Dissolution Kinetics and Biodurability of Tremolite Particles in Mimicked Lung Fluids: Effect of Citrate and Oxalate. *J. Asian Earth Sci.* **2013**, *77*, 318−326.
(19) Sauer, U. G.; Werle, K.; Waindok, H.; Hirth, S.; Hachmöller, O.; Wohlleben, W. Critical Choices in Predicting Stone Wool Biodurability: Lysosomal Fluid Compositions and Binder Effects. *Chem. Res. Toxicol.* **2021**, *34*, 780−792.
(20) Muhle, H.; Bellmann, B.; Sebastian, K.; Böhm, T.; Nies, E.; Barig, A.*Fasern - Tests Zur Abschätzung Der Biobeständigkeit Und Zum Verstaubungsverhalten (Fibres − Tests to Assess Biodurability and Dust Behaviour)*, 1998.
(21) Midander, K.; Pan, J.; Odnevall Wallinder, I.; Leygraf, C. Metal Release from Stainless Steel Particles in Vitro - Influence of Particle Size. *J. Environ. Monit.* **2007**, *9*, 74−81.
(22) Stefaniak, A. B.; Guilmette, R. A.; Day, G. A.; Hoover, M. D.; Breysse, P. N.; Scripsick, R. C. Characterization of Phagolysosomal Simulant Fluid for Study of Beryllium Aerosol Particle Dissolution. *Toxicol. In Vitro* **2005**, *19*, 123−134.
(23) Sergin, I.; Evans, T.; Razani, B. Degradation and beyond: The Macrophage Lysosome as a Nexus for Nutrient Sensing and Processing in Atherosclerosis. *Curr. Opin. Lipidol.* **2015**, *26*, 394−404.
(24) Sun-Wada, G. H.; Wada, Y.; Futai, M. Lysosome and Lysosome-Related Organelles Responsible for Specialized Functions in Higher Organisms, with Special Emphasis on Vacuolar-Type Proton ATPase. *Cell Struct. Funct.* **2003**, *28*, 455−463.
(25) Etherington, D. J.; Pugh, D.; Silver, I. A. Collagen Degradation in an Experimental Inflammatory Lesion: Studies on the Role of the Macrophage. *Acta Biol. Med. Ger.* **1981**, *40*, 1625−1636.
(26) Nyberg, K.; Johansson, U.; Johansson, A.; Camner, P. Phagolysosomal PH in Alveolar Macrophages. *Environ. Health Perspect.* **1992**, *97*, 149−152.
(27) Ohkuma, S.; Poole, B. Fluorescence Probe Measurement of the Intralysosomal PH in Living Cells and the Perturbation of PH by Various Agents. *Proc. Natl. Acad. Sci. U. S. A.* **1978**, *75*, 3327−3331.
(28) Weber, K.; Schilling, J. D. Distinct Lysosome Phenotypes Influence Inflammatory Function in Peritoneal and Bone Marrow-Derived Macrophages. *Int. J. Inflammation* **2014**, *2014*, 1.
(29) Sarafian, V. S.; Marinova, T. T. Lysosomal Membrane-Associated Glycoproteins Are Differentially Expressed in Acute and Chronic Human Thymic Involution. *Acta Biol. Hung.* **2006**, *57*, 315−322.
(30) Tappel, A. L.Chapter 9: Lysosomal Enzymes and Other Components. In *Lysosomes in Biology and Pathology*; North-Holland Publishing Company: Amsterdam − London, 1975.
(31) Arborgh, B.; Glaumann, H.; Berg, T.; Ericsson, J. L. E. Isolation of Kupffer Cell Lysosomes, with Observations on Their Chemical and Enzymic Composition. *Exp. Cell Res.* **1974**, *88*, 279−288.
(32) Berry, J. P. The Role of Lysosomes in the Selective Concentration of Mineral Elements. A Microanalytical Study. *Cell. Mol. Biol.* **1996**, *42*, 395−411.
(33) Christensen, K. A.; Myers, J. T.; Swanson, J. A. PH-Dependent Regulation of Lysosomal Calcium in Macrophages. *J. Cell Sci.* **2002**, *115*, 599−607.

(34) Köpf-Maier, P. The Phosphorus Content of Lysosomes in Hepatocytes and Kupffer Cells. *Cells Tissues Organs* **1990**, *139*, 164−172.
(35) Tapper, H.; Sundler, R. Role of Lysosomal and Cytosolic PH in the Regulation of Macrophage Lysosomal Enzyme Secretion. *Biochem. J.* **1990**, *272*, 407−414.
(36) Rider, E. D.; Pinkerton, K. E.; Jobe, A. H. Characterization of Rabbit Lung Lysosomes and Their Role in Surfactant Dipalmitoylphosphatidylcholine Catabolism. *J. Biol. Chem.* **1991**, *266*, 22522−22528.
(37) Lundborg, M.; Falk, R.; Johansson, A.; Kreyling, W.; Camner, P. Phagolysosomal PH and Dissolution of Cobalt Oxide Particles by Alveolar Macrophages. *Environ. Health Perspect.* **1992**, *97*, 153−157.
(38) Lundborg, M.; Johard, U.; Johansson, A.; Eklund, A.; Falk, R.; Kreyling, W.; Camner, P. Phagolysosomal Morphology and Dissolution of Cobalt Oxide Particles by Human and Rabbit Alveolar Macrophages. *Exp. Lung Res.* **1995**, *21*, 51−66.
(39) Oh, Y. K.; Swanson, J. A. Different Fates of Phagocytosed Particles after Delivery into Macrophage Lysosomes. *J. Cell Biol.* **1996**, *132*, 585−593.
(40) Berry, J. P.; Zhang, L.; Galle, P.; Ansoborlo, E.; Hengé-Napoli, M. H.; Donnadieu-Claraz, M. Role of Alveolar Macrophage Lysosomes in Metal Detoxification. *Microsc. Res. Tech.* **1997**, *36*, 313−323.
(41) Wan, B.; Wang, Z. X.; Lv, Q. Y.; Dong, P. X.; Zhao, L. X.; Yang, Y.; Guo, L. H. Single-Walled Carbon Nanotubes and Graphene Oxides Induce Autophagosome Accumulation and Lysosome Impairment in Primarily Cultured Murine Peritoneal Macrophages. *Toxicol. Lett.* **2013**, *221*, 118−127.
(42) Shinohara, N.; Zhang, G.; Oshima, Y.; Kobayashi, T.; Imatanaka, N.; Nakai, M.; Sasaki, T.; Kawaguchi, K.; Gamo, M. Kinetics and Dissolution of Intratracheally Administered Nickel Oxide Nanomaterials in Rats. *Part. Fibre Toxicol.* **2017**, *14*, 1−14.
(43) Stopford, W.; Turner, J.; Cappellini, D.; Brock, T. Bioaccessibility Testing of Cobalt Compounds. *J. Environ. Monit.* **2003**, *5*, 675−680.
(44) Zoitos, B. K.; De Meringo, A.; Rouyer, E.; Bauer, S. T. J.; Law, B.; Boymel, P. M.; Olson, J. R.; Christensen, V. R.; Guldberg, M.; Koenig, A. R.; Perander, M. In Vitro Measurement of Fiber Dissolution Rate Relevant to Biopersistence at Neutral PH: An Interlaboratory Round Robin. *Inhalation Toxicol.* **1997**, *9*, 525−540.
(45) Li, J.; Zhang, W.; Zhu, J.; Lu, J. The Influence of Citrate on Surface Dissolution and Alteration of the Micro- and Nano-Structure of Biotite. *RSC Adv.* **2016**, *6*, 112544−112551.
(46) Thelohan, S.; De Meringo, A. In Vitro Dynamic Solubility Test: Influence of Various Parameters. *Environ. Health Perspect.* **1994**, *102*, 91−96.
(47) Liu, X.; Hurt, R. H.; Kane, A. B. Biodurability of Single-Walled Carbon Nanotubes Depends on Surface Functionalization. *Carbon* **2010**, *48*, 1961−1969.
(48) Allen, B. L.; Kichambare, P. D.; Gou, P.; Vlasova, I. I.; Kapralov, A. A.; Konduru, N.; Kagan, V. E.; Star, A. Biodegradation of Single-Walled Carbon Nanotubes through Enzymatic Catalysis. *Nano Lett.* **2008**, *8*, 3899−3903.
(49) Russier, J.; Ménard-Moyon, C.; Venturelli, E.; Gravel, E.; Marcolongo, G.; Meneghetti, M.; Doris, E.; Bianco, A. Oxidative Biodegradation of Single- and Multi-Walled Carbon Nanotubes. *Nanoscale* **2011**, *3*, 893−896.
(50) Yokel, R. A.; Hancock, M. L.; Grulke, E. A.; Unrine, J. M.; Dozier, A. K.; Graham, U. M. Carboxylic Acids Accelerate Acidic Environment-Mediated Nanoceria Dissolution. *Nanotoxicology* **2019**, *13*, 455−475.
(51) Marques, M. R. C.; Loebenberg, R.; Almukainzi, M. Simulated Fluids. *Dissolution Technol.* **2011**, *18*, 15−28.
(52) Walczak, A. P.; Fokkink, R.; Peters, R.; Tromp, P.; Herrera Rivera, Z. E.; Rietjens, I. M. C. M.; Hendriksen, P. J. M.; Bouwmeester, H. Behaviour of Silver Nanoparticles and Silver Ions in an in Vitro Human Gastrointestinal Digestion Model. *Nanotoxicology* **2012**, *7*, 1198−1210.
(53) Llewellyn, S. V.; Conway, G. E.; Zanoni, I.; Jørgensen, A. K.; Shah, U. K.; Seleci, D. A.; Keller, J. G.; Kim, J. W.; Wohlleben, W.; Jensen, K. A.; Costa, A.; Jenkins, G. J. S.; Clift, M. J. D.; Doak, S. H. Understanding the Impact of More Realistic Low-Dose, Prolonged Engineered Nanomaterial Exposure on Genotoxicity Using 3D Models of the Human Liver. *J. Nanobiotechnol.* **2021**, *19*, 1−24.
(54) Konduru, N.; Keller, J.; Ma-Hock, L.; Gröters, S.; Landsiedel, R.; Donaghey, T. C.; Brain, J. D.; Wohlleben, W.; Molina, R. M. Biokinetics and Effects of Barium Sulfate Nanoparticles. *Part. Fibre Toxicol.* **2014**, *11*, 1−15.
(55) Wohlleben, W.; Ma-Hock, L.; Boyko, V.; Cox, G.; Egenolf, H.; Freiberger, H.; Hinrichsen, B.; Hirth, S.; Landsiedel, R. Nanospecific Guidance in REACH: A Comparative Physical-Chemical Characterization of 15 Materials with Methodical Correlations. *J. Ceram. Sci. Technol.* **2013**, *4*, 93−104.
(56) Singh, C.; Friedrichs, S.; Levin, M.; Birkedal, R.; Jensen, K. A.; Pojana, G.; Wohlleben, W.; Schulte, S.; Wiench, K.; Turney, T.; Koulaeva, O.; Marshall, D.; Hund-Rinke, K.; Kördel, W.; Van Doren, E.; De Temmerman, P.-J.; Abi, M.; Francisco, D.; Mast, J.; Gibson, N.; Koeber, R.; Linsinger, T.; Klein, C. L.*NM-Series of Representative Manufactured Nanomaterials Characterisation and Test Item Preparation*, 2011.
(57) Koltermann-Jülly, J.; Keller, J. G.; Vennemann, A.; Werle, K.; Müller, P.; Ma-Hock, L.; Landsiedel, R.; Wiemann, M.; Wohlleben, W. Abiotic Dissolution Rates of 24 (Nano)Forms of 6 Substances Compared to Macrophage-Assisted Dissolution and in Vivo Pulmonary Clearance: Grouping by Biodissolution and Transformation. *NanoImpact* **2018**, *12*, 29−41.
(58) Keller, J. G.; Graham, U. M.; Koltermann-Jülly, J.; Gelein, R.; Ma-Hock, L.; Landsiedel, R.; Wiemann, M.; Oberdörster, G.; Elder, A.; Wohlleben, W. Predicting Dissolution and Transformation of Inhaled Nanoparticles in the Lung Using Abiotic Flow Cells: The Case of Barium Sulfate. *Sci. Rep.* **2020**, *10*, 1−15.
(59) Keller, J. G.; Peijnenburg, W.; Werle, K.; Landsiedel, R.; Wohlleben, W. Understanding Dissolution Rates via Continuous Flow Systems with Physiologically Relevant Metal Ion Saturation in Lysosome. *Nanomaterials* **2020**, *10*, 1−16.
(60) Keller, J. G.; Persson, M.; Müller, P.; Ma-Hock, L.; Werle, K.; Arts, J.; Landsiedel, R.; Wohlleben, W. Variation in Dissolution Behavior among Different Nanoforms and Its Implication for Grouping Approaches in Inhalation Toxicity. *NanoImpact* **2021**, *23*, No. 100341.
(61) Guldberg, M.; Madsen, A. L.; Sebastian, K.; Fellmann, J.; Potter, R.; Bauer, J.; Searl, A.; Maquin, B.; Jubb, G. In-Vitro Dissolution of Vitreous Silicate Fibres According to EURIMA Test Guideline - Results of Two Round Robins. *Glass Sci. Technol.* **2003**, *76*, 199−205.
(62) Wagner, T.*Ij-Particlesizer: ParticleSizer 1.0.1*; Zenodo, 2016.
(63) Verleysen, E.; Wagner, T.; Lipinski, H.-G.; Kägi, R.; Koeber, R.; Boix-Sanfeliu, A.; De Temmerman, P.-J.; Mast, J. Evaluation of a TEM Based Approach for Size Measurement of Particulate (Nano)Materials. *Materials* **2019**, *12*, 2274.
(64) Choi, E.; Kim, S. Surface PH Buffering to Promote Degradation of Mesoporous Silica Nanoparticles under a Physiological Condition. *J. Colloid Interface Sci.* **2019**, *533*, 463−470.
(65) Gorrepati, E. A.; Wongthahan, P.; Raha, S.; Fogler, H. S. Silica Precipitation in Acidic Solutions: Mechanism, PH Effect, and Salt Effect. *Langmuir* **2010**, *26*, 10467−10474.
(66) Metin, C. O.; Bonnecaze, R. T.; Lake, L. W.; Miranda, C. R.; Nguyen, Q. P. Aggregation Kinetics and Shear Rheology of Aqueous Silica Suspensions. *Appl. Nanosci.* **2014**, *4*, 169−178.
(67) Kobayashi, M.; Juillerat, F.; Galletto, P.; Bowen, P.; Borkovec, M. Aggregation and Charging of Colloidal Silica Particles: Effect of Particle Size. *Langmuir* **2005**, *21*, 5761−5769.
(68) Kumar, S.; Aswal, V. K.; Callow, P. PH-Dependent Interaction and Resultant Structures of Silica Nanoparticles and Lysozyme Protein. *Langmuir* **2014**, *30*, 1588−1598.
(69) Bermudez, E.; Mangum, J. B.; Wong, B. A.; Asgharian, B.; Hext, P. M.; Warheit, D. B.; Everitt, J. I. Pulmonary Responses of Mice, Rats, and Hamsters to Subchronic Inhalation of Ultrafine Titanium Dioxide Particles. *Toxicol. Sci.* **2004**, *77*, 347−357.
(70) Landsiedel, R.; Ma-Hock, L.; Kroll, A.; Hahn, D.; Schnekenburger, J.; Wiench, K.; Wohlleben, W. Testing Metal-Oxide Nanomaterials for Human Safety. *Adv. Mater.* **2010**, *22*, 2601−2627.

https://doi.org/10.1021/acs.chemrestox.1c00418
Chem. Res. Toxicol. 2022, 35, 963−980

(71) Landsiedel, R.; Ma-Hock, L.; Hofmann, T.; Wiemann, M.; Strauss, V.; Treumann, S.; Wohlleben, W.; Gröters, S.; Wiench, K.; Van Ravenzwaay, B. Application of Short-Term Inhalation Studies to Assess the Inhalation Toxicity of Nanomaterials. *Part. Fibre Toxicol.* **2014**, *11*, 16.
(72) Molina, R. M.; Konduru, N. V.; Jimenez, R. J.; Pyrgiotakis, G.; Demokritou, P.; Wohlleben, W.; Brain, J. D. Bioavailability, Distribution and Clearance of Tracheally Instilled, Gavaged or Injected Cerium Dioxide Nanoparticles and Ionic Cerium. *Environ. Sci. Nano* **2014**, *1*, 561−573.
(73) Janer, G.; Ag-Seleci, D.; Sergent, J. A.; Landsiedel, R.; Wohlleben, W. Creating Sets of Similar Nanoforms with the ECETOC NanoApp: Real-Life Case Studies. *Nanotoxicology* **2021**, *15*, 1−1034.
(74) Janer, G.; Landsiedel, R.; Wohlleben, W. Rationale and Decision Rules behind the ECETOC NanoApp to Support Registration of Sets of Similar Nanoforms within REACH. *Nanotoxicology* **2021**, *15*, 145−166.
(75) Rasmussen, K.; Mech, A.; Mast, J.; De Temmerman, P.-J.; Waegeneers, N.; Van Steen, F.; Pizzolon, J. C.; De Temmerman, L.; Van Doren, E.; Jensen, K. A.; Birkedal, R.; Levin, M.; Nielsen, S. H.; Koponen Ismo, K.; Clausen, P. A.; Kembouche, Y.; Thieriet, N.; Spalla, O.; Giuot, C.; Rousset, D.; Witschger, O.; Bau, S.; Bianchi, B.; Shivachev, B.; Gilliland, D.; Pianella, F.; Ceccone, G.; Cotogno, G.; Rauscher, H.; Gibson, P.; Stamm, H.*Synthetic Amorphous Silicon Dioxide (NM-200, NM-201, NM-202, NM-203, NM-204): Characterisation and Physico-Chemical Properties*; 2013.
(76) Farcal, L.; Andón, F. T.; Di Cristo, L.; Rotoli, B. M.; Bussolati, O.; Bergamaschi, E.; Mech, A.; Hartmann, N. B.; Rasmussen, K.; Riego-Sintes, J.; Ponti, J.; Kinsner-Ovaskainen, A.; Rossi, F.; Oomen, A.; Bos, P.; Chen, R.; Bai, R.; Chen, C.; Rocks, L.; Fulton, N.; Ross, B.; Hutchison, G.; Tran, L.; Mues, S.; Ossig, R.; Schnekenburger, J.; Campagnolo, L.; Vecchione, L.; Pietroiusti, A.; Fadeel, B. Comprehensive in Vitro Toxicity Testing of a Panel of Representative Oxide Nanomaterials: First Steps towards an Intelligent Testing Strategy. *PLoS One* **2015**, *10*, 1−34.
(77) Pavan, C.; Delle Piane, M.; Gullo, M.; Filippi, F.; Fubini, B.; Hoet, P.; Horwell, C. J.; Huaux, F.; Lison, D.; Lo Giudice, C.; Martra, G.; Montfort, E.; Schins, R.; Sulpizi, M.; Wegner, K.; Wyart-Remy, M.; Ziemann, C.; Turci, F. The Puzzling Issue of Silica Toxicity: Are Silanols Bridging the Gaps between Surface States and Pathogenicity? *Part. Fibre Toxicol.* **2019**, *16*, 1−10.
(78) Chen, J.; Li, J.; Zhou, J.; Lin, Z.; Cavalieri, F.; Czuba-Wojnilowicz, E.; Hu, Y.; Glab, A.; Ju, Y.; Richardson, J. J.; Caruso, F. Metal-Phenolic Coatings as a Platform to Trigger Endosomal Escape of Nanoparticles. *ACS Nano* **2019**, *13*, 11653−11664.
(79) Donahue, N. D.; Acar, H.; Wilhelm, S. Concepts of Nanoparticle Cellular Uptake, Intracellular Trafficking, and Kinetics in Nanomedicine. *Adv. Drug Delivery Rev.* **2019**, *143*, 68−96.
(80) Iler, R. K.*The Chemistry of Silica Solubility, Polymerization, Colloid and Surface Properties, and Biochemistry of Silica*, 1979.
(81) Innes, E.; Yiu, H. H. P.; McLean, P.; Brown, W.; Boyles, M. Simulated Biological Fluids−a Systematic Review of Their Biological Relevance and Use in Relation to Inhalation Toxicology of Particles and Fibres. *Crit. Rev. Toxicol.* **2021**, *51*, 217−248.
(82) Barly, S. H. Q.; Okhrimenko, D. V.; Solvang, M.; Yue, Y.; Stipp, S. L. S. Dissolution of Stone Wool Fibers with Phenol-Urea-Formaldehyde Binder in a Synthetic Lung Fluid. *Chem. Res. Toxicol.* **2019**, *32*, 2398−2410.
(83) Finch, G. L.; Mewhinney, J. A.; Hoover, M. D.; Eidson, A. F.; Haley, P. J.; Bice, D. E. Clearance, Translocation, and Excretion of Beryllium Following Acute Inhalation of Beryllium Oxide by Beagle Dogs1. *Toxicol. Sci.* **1990**, *15*, 231−241.
(84) Jeong, J.; Kim, J.; Seok, S. H.; Cho, W. S. Indium Oxide (In2O3) Nanoparticles Induce Progressive Lung Injury Distinct from Lung Injuries by Copper Oxide (CuO) and Nickel Oxide (NiO) Nanoparticles. *Arch. Toxicol.* **2016**, *90*, 817−828.
(85) Adamcakova-Dodd, A.; Stebounova, L. V.; Kim, J. S.; Vorrink, S. U.; Ault, A. P.; O'Shaughnessy, P. T.; Grassian, V. H.; Thorne, P. S. Toxicity Assessment of Zinc Oxide Nanoparticles Using Sub-Acute and Sub-Chronic Murine Inhalation Models. *Part. Fibre Toxicol.* **2014**, *11*, 1−15.
(86) Latvala, S.; Hedberg, J.; Di Bucchianico, S.; Möller, L.; Odnevall Wallinder, I.; Elihn, K.; Karlsson, H. L. Nickel Release, ROS Generation and Toxicity of Ni and NiO Micro- and Nanoparticles. *PLoS One* **2016**, *11*, e0159684−e0159684.
(87) Berry, J. P. The Role of Lysosomes in the Selective Concentration of Mineral Elements. A Microanalytical Study. *Cell. Mol. Biol.* **1996**, *42*, 395−411.
(88) Boisa, N.; Elom, N.; Dean, J. R.; Deary, M. E.; Bird, G.; Entwistle, J. A. Development and Application of an Inhalation Bioaccessibility Method (IBM) for Lead in the PM10 Size Fraction of Soil. *Environ. Int.* **2014**, *70*, 132−142.
(89) International Agency for Research on Cancer. International Agency for Research on Cancer Iarc Monographs on the Evaluation of Carcinogenic Risks To Humans. *Iarc Monogr. Eval. Carcinog. Risks To Humansarc Monogr. Eval. Carcinog. Risks To Humans*, 2002, *96*, i-ix+1-390.
(90) I.A.F.R.O.C. IARC. *WORLD HEALTH ORGANIZATION*, 2002.
(91) Guldberg, M.*Annals of Occupational Hygiene*, 1998.
(92) Sauer, U. G.; Werle, K.; Waindok, H.; Hirth, S.; Hachmöller, O.; Wohlleben, W. Reply to the Comment on Critical Choices in Predicting Stone Wool Biodurability: Lysosomal Fluid Compositions and Binder Effects. *Chem. Res. Toxicol.* **2021**, *34*, 1697−1698.

https://doi.org/10.1021/acs.chemrestox.1c00418
Chem. Res. Toxicol. 2022, 35, 963−980